Titel
Title

Surface Treatment for Additive Manufactured Aluminum Alloys

Författare
Author

Karin Andersson
Marianne Gavelius

Sammanfattning
Abstract

Manufacturing of aircraft parts is often complex and time-consuming, which has led to an increased interest in new manufacturing technologies in the Swedish industry such as additive manufacturing (AM). Additive manufacturing techniques could be a solution to meet the aircrafts' demand since it contributes to an efficient manufacturing and allows a just-in-time production of complex metal parts in their final shape. However, the use of AM aluminum for aircraft applications is in a development phase and no surface treatment process exists. Thereby, it is of high interest to further investigate surface treatments for AM alloys. Currently at Saab AB, conventional aluminum alloys are generally anodized in tartaric sulphuric acid (TSA) to improve the corrosion resistance and adhesion properties of the metal. On the behalf of Saab AB, there is also an interest in establishing powder coating as a surface treatment.

This master thesis' purpose is to investigate the anodizing and adhesion properties for the two additive manufacturing alloys - AlSi10Mg and Scalmalloy®, and compare it with the conventionally produced Al alloy 2024-T3. The anodization and the powder coating is examined by using following characterization techniques: profilometry, light microscopy, scanning electron microscopy and contact angle measurements. The results from the experimental part indicated successful anodizations for all the alloys and good adhesion properties for powder coating. This research is a first step in contributing to a better understanding of the anodic coating and adhesion properties for the AM samples Scalmalloy® and AlSi10Mg.

Nyckelord
Keyword

Surface treatment, additive manufacturing, Al alloy 2024-T3, Scalmalloy, AlSi10Mg, powder coating, TSA, anodization, SEM

Surface Treatment for Additive Manufactured Aluminum Alloys

Final report 2020-06-04

Karin Andersson and Marianne Gavelius

Examiner: Kajsa Uvdal (IFM)
Supervisors: Christian Ulrich (Saab), Linnéa Selegård (Saab/IFM) and Zhangjun Hu (IFM)

Abstract

Manufacturing of aircraft parts is often complex and time-consuming, which has led to an increased interest in new manufacturing technologies in the Swedish industry such as additive manufacturing (AM). Additive manufacturing techniques could be a solution to meet the aircrafts' demand since it contributes to an efficient manufacturing and allows a just-in-time production of complex metal parts in their final shape. However, the use of AM aluminum for aircraft applications is in a development phase and no surface treatment process exists. Thereby, it is of high interest to further investigate surface treatments for AM alloys. Currently at Saab AB, conventional aluminum alloys are generally anodized in tartaric sulphuric acid (TSA) to improve the corrosion resistance and adhesion properties of the metal. On the behalf of Saab AB, there is also an interest in establishing powder coating as a surface treatment.

This master thesis' purpose is to investigate the anodizing and adhesion properties for the two additive manufacturing alloys - AlSi10Mg and Scalmalloy$^{®}$, and compare it with the conventionally produced Al alloy 2024-T3. The anodization and the powder coating are examined by using following characterization techniques: profilometry, light microscopy, scanning electron microscopy and contact angle measurements. The results from the experimental part indicated successful anodizations for all the alloys and good adhesion properties for powder coating. This research is a first step in contributing to a better understanding of the anodic coating and adhesion properties for the AM samples Scalmalloy$^{®}$ and AlSi10Mg.

Keywords: surface treatment, additive manufacturing, Al alloy 2024-T3, Scalmalloy$^{®}$, AlSi10Mg, powder coating, TSA, anodization, SEM

Acknowledgement

List of abbreviations

AM - Additive manufacturing
BSE - Backscattered Electron
CA - Contact Angle
CAM - Contact Angle Measurement
IFM - department of Physics, Chemistry and Biology
LiU - Linköping University
L-PBF - Laser-Powder Bed Fusion
REACH - Registration, Evaluation, Authorization and restriction of Chemicals
SE - Secondary Electrons
SEM - Scanning Electron Microscopy

Chemical Denotations

Al - Aluminum
Al_2O_3 - Alumina, Aluminum Oxide
Cr - Chromium
Cr(III) - Trivalent chromium
Cr(VI) - Hexavalent chromium
Cu - Copper
H_2O_2 - Hydrogen Peroxide
Fe - Iron
Mn - Manganese
Mg - Magnesium
PA - Phosphoric Acid
Pt - Platinum
SA - Sulphuric Acid
Sc - Scandium
Si - Silicon
Ti - Titanium
TSA - Tartaric Sulphuric Acid
Zn - Zinc
Zr - Zirconium

Table of contents

1 | Introduction

In the aerospace industry, it is of high importance that the material in use has a high strength to weight ratio, durability, and good properties such as corrosion resistance. Manufacturing of aircraft parts is often complex and time-consuming, therefore there is an interest in new manufacturing techniques such as additive manufacturing (AM). AM could allow a just-in-time production and production of metal parts in their final complex shape. However, the use of additive manufactured aluminum for aircraft is in a development phase and there exist no surface treatments.

The most widely used material in aerospace industries are aluminum alloys, and to create desirable durability and corrosion resistance for the alloys, surface treatment is required. One frequently used process is anodization, an electrochemical surface treatment applied to aluminum alloys to protect it against corrosion. The anodization process improves the corrosion resistance by developing a protective oxide layer consisting of alumina (Al_2O_3) with porous morphology.(Thompson *et al*., 1999) Anodization using hexavalent chromium was previously commonly used due to its efficiency to produce oxide layers and for its corrosion resistance - but the use is strictly regulated due to its carcinogenic and toxic nature and there is a need to reduce these harmful substances. Today, the use of tartaric sulphuric acid (TSA) is adapted in the aircraft industry, including Saab AB (Critchlow *et al*., 2006). Anodizing with TSA has been widely investigated for the common aluminum alloy 2024-T3, but further investigations for other alloys such as AM alloys, is of great interest since AM aluminum alloys are not used in the aircraft industry due to a lack of knowledge about its surface treatment. If anodizing with TSA can be proven for AM aluminum alloys, AM aluminum alloys may be useful for future projects in the aircraft industry in order to enable a more time-consuming production.

In addition to anodization, it is common for surfaces to be treated with wet paint to improve corrosion resistance. Unfortunately, most of the paints used contain solvents and hexavalent chromium, which is carcinogenic and toxic (Vargel, 2004; Valdesueiro *et al*., 2017). Consequently, other methods such as powder coating are of interest. Powder coating is an interesting method to investigate for several aluminum alloys since it is considered more resistant to corrosion, chemicals and weather than conventional solvent-based wet paint (Sharifi *et al*., 2017). Powder coating is not used on a daily basis in aerospace applications but due to the advantages of the method, powder coating may be useful for future projects in the aircraft industry.

1.1 Purpose

The purpose of this master thesis is to compare the anodizing properties of two different AM alloys, AlSi10Mg and Scalmalloy®, with the conventionally produced aluminum alloy 2024-T3. This comparison has not yet been executed and this will be done by studying the porosity and wettability of the oxide layer obtained by anodization. The surfaces are characterized using tools such as light microscope, contact angle goniometry and scanning electron microscopy. There is also an interest in investigating blasted alloys, since a comparison in surface treatment of raw and blasted alloys have not been discovered before. Further, an investigation of the behaviors of powder coating on the anodized AM parts is conducted since this has not been done before. In summary, this project contributes to a better understanding of the anodic coating properties and powder coating of AM parts in order to enable the use of AM parts in the aircraft industry.

1.2 Delimitations

When implementing the project, limitations in method, materials, and instruments will be made. The conventionally produced aluminum alloy 2024-T3 is widely known and its properties are well understood for the aerospace industry. Aluminum alloy 2024-T3 is commonly used at Saab AB today, thereby this alloy will be used as a reference for this project as well. AlSi10Mg is a common alloy that has been used for similar industries as for Saab AB. Consequently, it is of interest to investigate AlSi10Mg properties for Saab AB's business, and therefore AlSi10Mg will be investigated in this project. Scalmalloy® is a high strength alloy that Saab AB finds very interesting to further investigate, thereby Scalmalloy® will be used for this project.

As for surface treatment, the aircraft industry wants to avoid wet paint to the greatest extent possible due to its solvents. There is an interest in investigating powder coating on AM parts. At Saab AB, a korroprimer is qualified for powder coating, thereby such product will be used for this project as well when performing the surface treatment. Some instruments have an hourly cost when using, therefore there is a restriction in the number of samples tested. During the master thesis, the world and Sweden were affected by a pandemic. Because of the virus COVID-19, the project was forced to be delimited since the accesses to premises, resources and instruments were regulated.

1.3 Collaboration Partners

This master thesis is executed in collaboration between the division Aeronautics - material and process technique at Saab AB with the division of Molecular Surface Physics and Nanoscience at Linköping University (LiU). The master thesis is executed by two students at LiU, studying Engineering Biology. One supervisor is from Aeronautics - material and process technique at Saab AB the other supervisors are from LiU. This is a bridging between industry and academia which makes it possible to gather important knowledge, information transfer, data collection and

analysis, as well as assistance needed to carry out the project. The Examiner for this master thesis is the head of division of Molecular Surface Physics and Nanoscience at IFM, the department of Physics, Chemistry, and Biology LiU.

1.3.1 Division of Molecular Surface Physics and Nanoscience

LiU is one of the largest universities in Sweden and consists of four faculties - Arts and Sciences, Educational Sciences, Medicine and Health Sciences, and the Institute of Technology. The faculties are divided into 14 departments, which in turn are divided into different areas. At LiU, this master thesis will take place at the department of IFM, in the field of Applied Physics at the division of Molecular Surface Physics and Nanoscience.

1.3.2 Saab AB

Saab AB is a Swedish aerospace and defense company. It was founded in 1937 and since then the company has grown and established itself globally. In Sweden, Saab AB is located in 27 cities, where Linköping is one of them. This master thesis is conducted in collaboration with Saab AB, Business area Aeronautics in Linköping. Aeronautics is one of six business areas within Saab AB and has a focus on developing JAS 39 Gripen. In this project, the methods used will closely mimic Saab AB's methods to obtain results that represent their production. Therefore, Saab AB will provide the material needed for the experiments in this project.

1.4 Expected impact of study

New insights regarding surface treatment for additive manufactured alloys can, in the long run, change today's manufacturing processes in the aircraft industry. Successful surface treatment for AM alloys enables the aircraft industry to use AM alloys in order to produce spare parts on demand. AM is a time-saving manufacturing technique and the amount of waste is reduced compared to conventionally produced spare parts. Results from an investigation of surface treatment of AM alloys has not yet been studied. By completing this project, a first insight into surface treatments of AM alloys in the aerospace industry will be received, new knowledge will be obtained, and possible process changes may become apparent. Since powder coating on AM alloys are yet to be established the results may prove to be knowledge rewarding and further projects might take place from this.

1.5 Project objectives

The main objectives of this project are to compare the anodization and powder coating properties of two different AM alloys; AlSi10Mg and Scalmalloy$^{®}$ with the conventionally produced aluminum alloy 2024-T3. These main objectives can be divided into four sub-projects:

1. The effect of the anodizing process of the aluminum alloy AlSi10Mg and Scalmalloy® will be investigated by using aluminum alloy 2024-T3 as a reference. The morphology of the anodic coating and roughness will be determined by using characterization methods such as light microscope, SEM, and profilometry.

2. The trends in wettability of the AM alloys compared to the reference material aluminum alloy 2024-T3 will be investigated. The wettability of anodized aluminum alloy samples will be determined by using contact angle goniometry.

3. The adhesion properties of powder coating on anodized AM alloys and aluminum alloy 2024-T3 will be investigated. The adhesion properties will be studied by performing three adhesion tests according to Saab AB's standard.

4. The effect of anodization of raw and blasted AM samples will be compared in order to investigate the difference in morphology of the anodic coating and the adhesion properties for different pre-treatments. The morphology of the anodic coating will be studied by using characterization methods such as light microscope, SEM, and profilometry. The adhesion properties will be studied by performing three adhesion tests according to Saab AB's standard.

2 | Scientific Background

In this chapter, the scientific background for this master thesis is presented. A description of the used aluminum alloys, surface treatments and powder coating will be presented. Furthermore, the explanatory theory on how substances are regulated, and biological effects will be discussed and illustrated.

2.1 Conventional aluminum alloys

Aluminum (Al) is an ideal choice to use in the automotive and aerospace industry since it has beneficial characteristic properties such as strength, stiffness, and good formability. Thereby, the use of Al reduces the weight which in turn leads to lower energy consumption and more fuel-efficiency. However, to reinforce the mechanical strength of Al and use it for structural parts, the Al is often alloyed with one or several elements. (Miller *et al.*, 2000; Cabrini *et al.*, 2016)

There are several manufacturing processes of Al alloys. Thus, Al alloys are divided into two categories: cast composition and wrought compositions. Cast alloys are produced using different casting techniques, and wrought alloys are produced by rolling, forging or extrusion. (Veys-Renaux *et al.,* 2016). Wrought Al alloys are designated by a four-digit numerical system called Alloy Designation System (IADS), which is developed by the Aluminum Association. Al alloys are thereby categorized in series depending on composition and are represented by four digits. The alloys from the 2XXX-series are the most commonly used in the aircraft industry. These alloys are hardened, and the main alloying element is Copper (Cu) (Mouritz, 2012).

In this master thesis, the wrought Al alloy 2024-T3 will be investigated and used as reference material due to the common use in Saab Aeronautics' aircraft production. The composition of Al alloy 2024-T3 is shown in Table 2.1. This alloy has Cu as the primary alloying element and is heat-treated to improve mechanical properties. During the heat treatment, the alloying elements react with Al which forms intermetallic precipitates that improves the strength and fatigue properties. The 2024-T3 Al alloy is often used in the aircraft industry for the wings and fuselage skins, which require high strength to weight ratio and good fatigue resistance. However, the 2024-T3 Al alloys do not have the perfect corrosion protection due to the alloying element Cu, and therefore need further surface treatments in order to improve corrosion resistance. (Mouritz, 2012; Kaushik, 2015)

Table 2.1. The composition [wt%] of the reference material Al alloy 2023-T3. The percentage composition of the alloying elements such as Copper (Cu), Magnesium (Mg), Manganese (Mn), Silicon (Si), Iron (Fe), Zink (Zn), Titanium (Ti), Chromium (Cr) and others. The composition of Al is balanced. (The Aluminum Association, 2015)

Al Alloy	Cu	Mg	Mn	Si	Fe	Zn	Ti	Cr	Others
2024-T3	3.8-4.9	1.2-1.8	0.3-0.9	≤ 0.5	≤ 0.5	0.25	≤ 0.15	≤ 0.1	≤ 0.15

2.2 Additive manufacturing

Manufacturing of aircraft parts is often complex and time consuming. Therefore, there is an interest in new manufacturing technologies for metal parts that are produced in the final required shape and size. One manufacturing technology that could meet the industry's needs could be additive manufacturing, also called 3D-printing. The first AM work was created in 1984, but the technology was expensive and unfeasible. However, during the 21st century, the costs decreased drastically, allowing the entry of 3D printers into many industries such as aerospace (Attaran, 2017). Additive manufacturing is a technique that builds objects by laying thin layers of material on top of each other. The technique is used to produce parts that have complex dimensions as the final required product. This enables production of more complex parts with a reduced weight compared to the conventional production techniques (Leon and Aghion, 2017).

It is crucial to find new ways to reduce the environmental impact of the manufacturing industry to further advance waste and energy reduction efforts. Research has shown that AM processes are more resource-efficient and will generate less waste than conventional manufacturing processes such as casting techniques. This results in more sustainable processes and smaller environmental footprints (Marcham and Walter, 2020). In the past few years, companies have embraced different AM technologies leading to remarkable progress in the advancements of AM. Different AM techniques allow building complex parts leading to shorter cycle time for manufacturing as well as material, energy and cost efficiency (Cabrini *et al.*, 2016). The aircraft industry has stringent regulations and manufacturing of aircraft parts is often time-consuming, leading to heavy inventory investment and hard to accomplish just-in-time production. AM is allowing a just-in-time production and resolvement of the supply chains and inventories (Singamneni *et al.*, 2019).

A strategic research agenda (SRA) was initiated by AMEXCI to attempt and clearly show that the Swedish manufacturing industry needs to take full advantage of the global AM movement. Saab AB is one of the companies supporting the SRA in order to develop and establish AM in the manufacturing industry. (Edström and Målberg, 2018)

2.2.1 Laser-Powder Bed Fusion

There exist different AM techniques and one is Laser-Powder Bed Fusion (L-PBF). L-PBF is a technique that applies a thin layer of powder material that is spread by a roller on the building platform. This process produces dense metal parts by using a high-power laser to melt and solidify the metal powder layer by layer. The first step is to design the required part, which results in a CAD-model. A high-power laser beam then fuses the Al alloy powder at the points defined by the CAD-model. Thereafter, the platform is lowered and another layer of powder is distributed on the top of the previous finished layer (Gardan, 2016)**.** The metal powder used is

pre-alloyed, and in combination with fast cooling rates, it promotes the formation of a fine microstructure and distribution of the alloying elements (Revilla *et al.,* 2019).

2.2.2 Additive manufactured Al alloys

In this thesis, the focus of the research is on the AM alloys AlSi10Mg and Scalmalloy®, and both alloys are produced by Laser-Powder Bed Fusion. The AlSi10Mg is produced by AMEXCI in a EOS M290 machine with layer thickness 30 μm. Scalmalloy® is produced by Fraunhofer EMI in Freiburg in a EOS M400 Single laser machine with layer thickness 60 μm. Silicon-containing Al cast alloys has been extensively used in the automotive and aerospace industry because of their high mechanical properties and corrosion resistance. The interest of AlSi10Mg alloy is because of the minor additions of magnesium (Mg), causing the hardening of the alloy. Thereby, the interest of AlSi10Mg has been increased due to its relatively high strength and stiffness to weight ratio (Revilla *et al.* 2019; Gu *et al.*, 2020). The composition of the different alloying elements in AlSi10Mg is presented in Table 2.2.

Table 2.2. *The composition [wt%] of AM AlSi10Mg. The percentage composition of the alloying elements such as Silicon (Si), Magnesium (Mg), Manganese (Mn), Titanium (Ti), Copper (Cu), Zink (Zn), Iron (Fe) and others. The composition of Al is balanced. (EOS M 290, n.d.)*

Al Alloy	Si	Mg	Mn	Ti	Cu	Zn	Fe	Others
AlSi10Mg	9 - 11	0.2-0.45	≤ 0.45	≤ 0.15	≤ 0.05	≤ 0.10	≤ 0.55	0.15

AlSi10Mg is a multiphase alloy, which means that the microstructure of AlSi10Mg alloy is composed of an α-Al phase, eutectic Si particles and secondary phases such as Mg2Si referred to β-phase. Research has been carried out to investigate the mechanical properties of the alloy and the results indicate that the eutectic Si particles degrade these properties (Gu *et al.*, 2020). The conditions during the AM process promote the formation of unique microstructures with fine internal phase distributions. This microstructure has a considerable influence on the corrosion and the anodizing mechanism (Revilla and De Graeve, 2018).

Saab AB is involved in the Clean sky 2 research programme that intends to develop and manufacture metallics with a focus on reducing the environmental impact of the aircraft industry (*Clean sky*, n.d.). In the Clean Sky 2 research programme, the potential use of different Al alloys currently available for additive manufacturing with L-PBF processes should be investigated. Fabrication and design guidelines as well as corresponding material properties are explored. Scalmalloy® is currently the most interesting new material for lightweight applications that are specifically developed for additive manufacturing. It has a high specific strength at the same time offering a reasonable amount of ductility, thus being potentially suitable for highly loaded functional parts. On behalf of Saab AB and their commitment to Clean Sky 2, there is a huge interest in investigating Scalmalloy®'s anodizing and adhesion properties. Scalmalloy® is

patented by APWorks and its properties are under investigation. This results in only limited research that can be found for this alloy.

Scalmalloy® has scandium (Sc) and magnesium (Mg) as the two main alloying elements. The chemical composition of Scalmalloy® is shown in Table 2.3. The interest of this alloy has increased due to its high-strength making it suitable for the automotive and aerospace industry (Schmidtke *et al.*, 2011). According to the manufacturer, Scalmalloy® has good fatigue properties and good anodization properties, making this alloy even more interesting to investigate further (apworks Home, n.d.).

Table 2.3. *The chemical composition [wt%] of Scalmalloy®. The percentage composition of the alloying elements such as Magnesium (Mg), Scandium (Sc), Zirconium (Zr), Manganese (Mn), Silicon (Si), Iron (Fe), Zink (Zn), Copper (Cu), Titanium (Ti) and others. The composition of Al is balanced.(Awd et al., 2017)*

Al Alloy	Mg	Sc	Zr	Mn	Si	Fe	Zn	Cu	Ti	Others
Scalmalloy®	4-4.9	0.6-0.8	0.2-0.5	0.3-0.8	≤0.4	≤0.4	≤0.25	≤0.1	≤0.15	≤0.10

2.2.3 Mechanical properties for AM metal parts

During the L-PBF process, high temperature and fast cooling cause residual stress in the metal part, which are adverse to their mechanical properties (Gu *et al.*, 2020; Bartlett and Li, 2019). The metal powder is rapidly heated up due to the absorption of the laser energy, which results in melt pools when the melting temperature is exceeded. The melt pools and the heat also affect surrounding zones of the metal powder causing the metal to be melted differently. This contributes to rough surfaces (Cheng and Chou, 2015). However, it is observed that AM metal parts have internal pores as a result of the AM process. This is critical for the aircraft industry since internal pores may contribute to high stress in the metal, making the metal unusable for the industry (Revilla *et al.,* 2019). Also, the rough surface is a great disadvantage of L-PBF, since the rough surface is suggested to affect the AlSi10Mg fatigue properties and also the corrosion resistance (Mower and Long, 2016; Kahlin *et al.*, 2017). It could be assumed that this could be the case for Scalmalloy® too, due to a similar manufacturing process for this alloy.

2.3 Corrosion of Al and Al alloys

Al alloys are widely used in the aerospace industry due to its high strength properties. Overall, pure Al has good corrosion resistance due to its natural protective oxide layer, but in environments under specific conditions corrosion may occur. When introducing alloying elements, the metal can be more prone to corrosion. Corrosion influences an alloy's durability by degrading the material's mechanical properties. Corrosion occurs when a metal is oxidized by an electrochemical reaction between the metal and an aqueous phase. For Al the mechanism of

corrosion is based on the oxidation of Al in an aqueous solution such as water (Vargel, 2004). This oxidation for Al proceeds as in the equation, Eq. (2.1) below.

$$Al \rightarrow Al^{3+} + 3e^{-} \qquad \text{Eq. (2.1)}$$
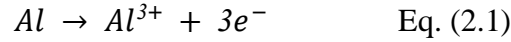
AM process results in the formation of unique microstructures and phase distributions that is different from the one obtained by conventional processing technologies (Leon and Aghion, 2017). These microstructures can have a considerable influence on the corrosion behavior and the mechanisms of surface treatments (Rubben *et al.*, 2019). The L-PBF process produces a rough surface that affects the surface properties of the parts, including corrosion properties. A study conducted by Leon and Aghion (2017) indicated that the corrosion resistance and fatigue life span of the L-PBF samples after polishing were improved compared to the unpolished samples. The reduced corrosion resistance and fatigue endurance of the unpolished L-PBF samples were related to their increased surface roughness and surface defects that are produced by the additive manufacturing process (Leon and Aghion, 2017). Therefore, finding a surface treatment for additive manufactured parts that increases the specimen's corrosion resistance becomes crucial. In automotive and aerospace applications, a common surface treatment of Al alloys to improve the corrosion resistance and the adhesion of paint coatings is anodizing (Vargel, 2004).

2.4 Anodization process

Surface treatment of Al alloys is done to improve the metal properties and prolong the durability. One frequently used method is anodizing, an electrochemical surface treatment applied to Al alloys to create protection against corrosion and improve adhesion properties (Vargel, 2004). The anodizing process is an electrochemical process which makes use of the Al's ability to develop a regular porous morphology (Thompson, 1999). During the anodization, the surface of the alloy is oxidized, and a protective, porous oxide coating is formed. This oxide coating is often called anodic coating (Vargel, 2004). The anodizing process involves an electrochemical cell with an anode, a cathode, a voltage source, and an electrolyte solution. (Abrahami *et al.*, 2017) The anodization is illustrated in Figure 2.1. The anode, an Al alloy, and the cathode are immersed in an electrolyte solution, which is electrically conducting. The anode is connected to the positive terminal of a voltage source and the cathode is connected to the negative terminal.
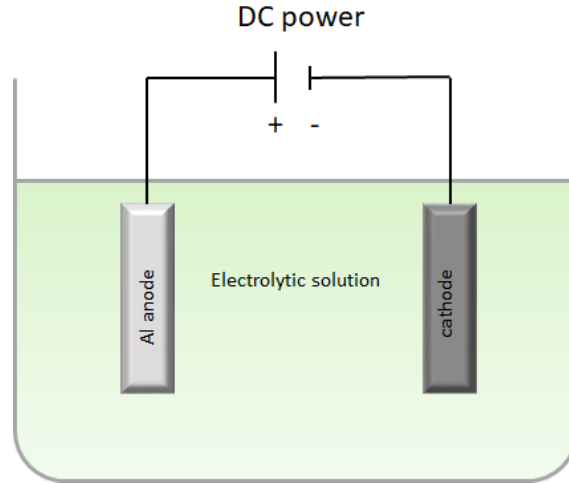
Figure 2.1: *An illustration of the anodization process. The Al alloy serves as an anode and is connected to the positive terminal of a DC power supply. The cathode is connected to the negative terminal.*

When applying the voltage to the system, the electrons are forced from the Al alloy which promotes the oxidation of Al atoms to Al cations (Al^{3+}) at the metal interface. The conductivity of the natural Al oxide is low, which results in the applied voltage encountering resistance by the existing oxide. This leads to different potential over the metal and electrolyte interface. The difference in potential enables the negatively charged anions of the electrolyte (O^{2-} and OH^-), to migrate to the positively charged anode. Thereby, a reaction between Al^{3+} and O^{2-} takes place and enables the formation of alumina (Al_2O_3) on the surface of the Al alloy, creating a reinforced oxide layer called anodic coating (Abrahami *et al.*, 2017; Zhu, 2019). The formation of this layer is described by the main reactions, Eq. 2.2 - 2.4 below.

$$2\ Al + 3\ H_2O \rightarrow Al_2O_3 + 3\ H_2 \qquad \text{Eq. (2.2)}$$

$$Al_2O_3 + 6\ H^+ \rightarrow 2\ Al^{3+} + 3\ H_2O \qquad \text{Eq. (2.3)}$$

$$3\ H_2O \rightarrow 6\ H^+ + 3\ O^{2-} \qquad \text{Eq. (2.4)}$$
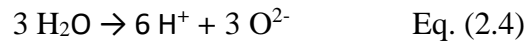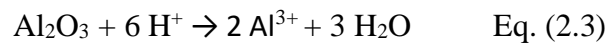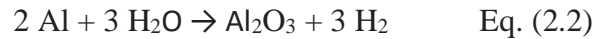
The anodizing process can be performed in different chemical solutions. However, acid solutions such as sulfuric acid are often used for surface treatment of Al (Abrahami *et al.*, 2017). At Saab AB, the acidic solution tartaric sulphuric acid (TSA) is used.

2.5 Morphology of the anodic coating

Depending on the electrolyte of choice, the oxide layer can consist of two parts, the barrier layer and the porous layer, which are illustrated in Figure 2.2. If the electrolyte solution is neutral, an uniform and compact oxide called the barrier layer is formed. However, when using an acidic or alkaline electrolyte the alumina layer can be dissolved. The oxide dissolves at the same pace as it

grows. Thereby, an oxide composed by two different alumina layers is generated. One alumina layer is the barrier layer and the other one is found on top of the barrier layer, called the porous layer. The porous layer is thicker, porous and has a characteristic hexagonal honeycomb structure. (Tommassi *et al.*, 2015; Thompson, 1997; Abrahami *et al.,* 2017)
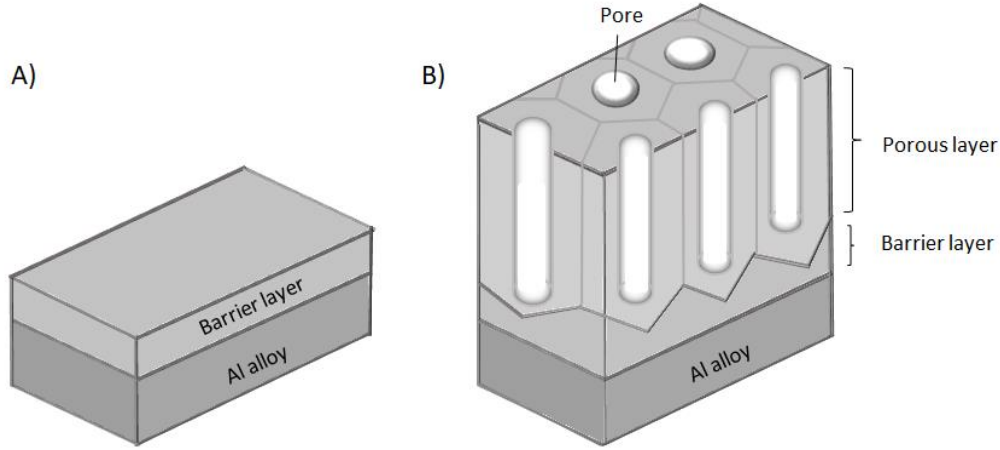
Figure 2.2: *Illustration of the two different formed alumina layers during the anodizing process, depending on electrolyte. A) Illustrates a created oxide film on Al when anodized in neutral electrolytes. B) Illustrates a created oxide film on Al when anodized in acidic electrolytes.*

The pore formation mechanism is still under investigation, but there are some basic theories. The generated porous morphology, when anodizing in acidic solutions, is the result of the electrochemical and chemical dissolution of alumina. It is believed that the pores are a result of the formed Al_2O_3 and the dissolution of O^{2-} and ejection of Al^{3+}, creating a penetration path. Depending on the penetration paths depth and width, pores are created. The reactions stated in Eq. 2.2-2.4 are stimulated by an electric field and the dissolution of the Al oxide. (Tommassi *et al.*, 2015)

The morphology of anodic coatings is often discussed in terms of pore organization (hexagonal), interpore distance, pore diameter, pore wall thickness and porosity, which is illustrated in Figure 2.3 (Tommassi *et al.*, 2015; Jani *et al.,* 2013). The term porosity is usually used to describe the morphology of the anodic coating by describing the fraction [%] of the pores on the coating (Ilango *et al.,* 2016). The porosity can also be described as a function of the pore diameter and pore wall thickness. The morphology of anodic coating can be modified and tuned by controlling anodization conditions such as applied voltage, electrolyte temperature and time. Thereby, the anodic coating parameters can be varied in a range of 10-400 nm for pore diameter, 50-600 nm for interpore distance and porosity from 5- 50 % (Jani *et al.,* 2013).
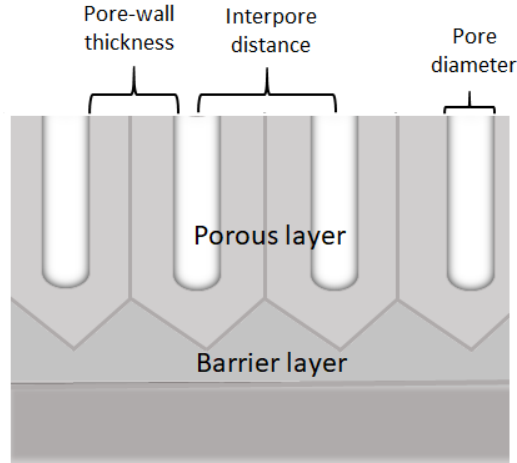
Figure 2.3: Illustrates the morphology of the anodic coating. The morphology is described by the parameters pore diameter, interpore distance and pore wall thickness.

2.6 Parameters affecting the anodic coating

Except for the electrolytes, other parameters affect the production of alumina. For the conventionally-produced Al alloys, the resulting porous structure is related to the anodization parameters such as voltage, current density, temperature and anodizing time (Vargel, 2004; Thompson *et al.*, 1999). By tuning the anodizing process parameters, the oxide thickness, pore diameter and porosity can be optimized depending on the final application. The oxide thickness largely depends largely on the applied voltage, thus the resulting current density. During the anodization, there will be an increased resistance of the coating build-up which will cause the current to gradually drop. Some studies have shown that an increasing current and thereby a larger current density provide a thicker barrier layer, improving the corrosion resistance of the alloy. There has also been reported that a higher applied current increases the pore diameters, which may improve the adhesion of paints and other finishing products (Abrahami *et al.*, 2017; Thompson, 1997).

The microstructure of the alloy will also play a crucial role in the formation and growth of the oxide layer. The microstructure of the alloy changes due to the intermetallic particles that are introduced by the presence of alloying elements. Thereby, the morphology of the formed anodized layers relies on the properties of the intermetallic particle. This could result in the anodic coating being less resistant making the alloy more prone to corrosion. (Veys-Renaux *et al.,* 2016; Li *et al.*, 2015)

2.6.1 Influence of alloying element

Due to the interest of AlSi10Mg in this master thesis, there is an interest to understand the influence of silicon on the anodization formation of anodic coating. In a study conducted by Zhu (2019), the anodizing behaviors of silicon-aluminum cast alloys were investigated and it was

suggested that silicon (Si) has a significant impact on the anodization. The Si-content and Si particle morphology influence the growth of the oxide layer. It was found that the formed oxide layer contains Si particles. This is probably a result of Si not being dissolved or anodized at the same rate as Al. The Si particles are embedded in the oxide layer and can act as a shield for the Al particles, preventing them from interacting with the electrolyte solution. The Al is thereby prevented from being anodized. In addition, it has also been shown that the anodization of silicon-aluminum cast alloys results in the formation of cavities above the Si particles. It is suggested that the oxidation of the Si particles is responsible for this. (Zhu *et al.*, 2016)

Another study conducted by Revilla et al. (2019), confirms that Si-particles have an impact on the anodic coating on additive manufactured AlSi10Mg. The study shows a decreasing oxide film growth, resulting in another structure of the formed oxide layer. It is suggested that the AM samples consumed a larger fraction of the anodic charge for the oxidation of the Si than for the conventional cast alloy with the corresponding chemical composition (Revilla *et al.*, 2019). In another study conducted by Revilla et al. (2017), the porous structure was found to be largely affected by the fine distribution of the silicon phase in the AlSi10Mg, leading to an increase of the pore diameter. The thickness of the oxide layer seems to depend on the amount of Si in silicon-aluminum alloys. A study conducted by Juhl (1998) shows that the oxide layer on AlSi0.5Mg is thicker than for AlSi7Mg and AlSi5Mg, and thereby concluded that the thickness of the oxide layer decreases by increasing Si concentration for cast Al-Si alloys.

Due to the interest of Scalmalloy® in this master thesis, there is an interest to understand the influence of magnesium (Mg) on the anodization. Results from anodizing Scalmalloy® have not been reported in literature. However, Mg alloys have been studied for anodizing in other conditions as for this project, such as different electrolytes and current density. Consequently, a comparison between this project and literature is challenging. Thereby, the influence of Mg under this project's conditions, such as anodization with TSA, is novel and important to investigate.

2.6.2 Influence of the microstructure and surface roughness

There are several manufacturing processes of Al alloys, and one process is casting. Depending on the casting process used, the microstructure of the Al alloy is changed. This results in varied properties of the anodic coating (Zhu, 2019). Other studies have found that pretreatment procedures such as annealing and polishing have an impact on the quality and pore properties of the oxide layer. During polishing, a flat and smooth surface of Al can be obtained. Thereby, the roughness of Al samples has an impact on the porous structure and it seems that an increasing roughness decreases the pore size of anodic Al oxide (Yu *et al.*, 2007). For AM metal parts, other factors such as surface roughness, the presence of unmelted powder on the surface and post-treatments such as blasting of the metal may also influence the morphology of the anodic oxide (Revilla *et al.,* 2019).

The anodization of AM Al alloys has not been studied to the same extent as cast and wrought alloys. However, there is some research that investigated the anodizing behavior of AM AlSi10Mg. According to a study conducted by Revilla et al. (2019), the anodic coating properties of AlSi10Mg are affected by the specific fine microstructure formed when undergoing the additive manufacturing process L-PBF. The study showed that the distribution of the Si phase caused the development of branched pores throughout the anodic oxide layer. It was also suggested that the microstructure of the Si phase has a higher impact on the anodic oxide growth than the amount of Si. The study also observes that the presence of internal pores in the AM samples forms cracks and thereby affects the anodic oxide layer. (Revilla *et al.,* 2019)

Scalmalloy® is an aluminum-magnesium-scandium alloy that is developed and patented by APWORKS. (apworks, n.d.) This alloy has also obtained a specific fine microstructure that is different from metals that have been produced by conventional production techniques. In comparison to the additive manufactured AlSi10Mg, there is no research available regarding Scalmalloy®'s anodizing properties. As mentioned earlier, the surface roughness and the alloying elements will affect the anodizing behaviors, and supposedly also in the case of Scalmalloy®. Due to the lack of knowledge of this AM alloy, there is a huge interest in investigating the anodic coating properties of this AM metal part.

2.7 REACH

REACH (Registration, Evaluation, Authorization and restriction of Chemicals) is a regulation that obligates companies and organizations to consider their use of chemicals. The regulation contains rules about manufacturing, import and sale of chemicals. In principle, all substances are covered by REACH regulation, making the use of chemicals more strictly regulated. When manufacturing or importing chemicals, a proper registration is needed. All compounds exceeding one ton when exporting must be tested with respect to health and environmental conditions. Depending on the toxicity of the substance, the usage can be limited, and special permission might be needed. Hexavalent chromium was normally used at Saab AB in its surface treatment process but has been regulated due to its toxicity and carcinogenesis effects. (*Swedish Chemical Agency*, n.d.)

2.8 Chromium and hexavalent chromium

Chromium (Cr) is a chemical element commonly used for surface treatments in the aerospace industry. In nature, Cr appears in chemical compounds, usually together with oxygen. Cr is present in several oxidation states where a difference in solubility, toxicity, bioavailability and mobility can be distinguished. It is a heavy metal that is one of the most common elements in the earth's crust. Heavy metals are often referred to as having a relatively high density and are toxic. However, it is of importance to know the quantity of the metal and its chemical state in order to

determine toxicity, since various chemical states have various toxicities. (Mishara and Bharagava, 2016)

The most common oxidation states of Cr are Cr(III) and Cr(VI) (Nationalencyklopedin, n.d.). Cr(III) has the capacity to interact with organic matter, making this form the most stable and less toxic one. As for biological activity, Cr(III) acts as an important nutrient to organic substances in soil and aquatic environments (Mishara and Bharagava, 2016). Also, Cr(III) is an essential micronutrient for human beings since it supports the lipid metabolism (Gupta, 2019). In comparison with Cr(III), Cr(VI) has a high mobility, solubility and is more toxic to the environment due to its capacity to form chromates (CrO_4^{2-}) and dichromates (CrO_7^{2-}) (Mishara and Bharagava, 2016). Chromates and dichromates are very toxic since it is absorbed into the body via both the lungs and the gastrointestinal tract. The capacity to form chromates and dichromates is favorable for the aerospace industry since it exhibits good corrosion resistance due to their ability to be either an anodic or a cathodic inhibitor. By being an anodic and a cathodic inhibitor at the same time, Cr(VI) can restrict the rate of metal dissolution and inhibit the oxygen and water reduction, contributing to good anti-corrosion protection (Gharbi *et al.*, 2018). However, the toxicity of Cr(VI) and its effects on humans need to be considered when using Cr-based surface treatments.

Cr(VI) is widely known as toxic and carcinogenic to humans since it is a strong oxidizing agent. Cr(VI) is very soluble in aqueous environments and due to its high solubility and strong oxidizing property, Cr(VI) has the possibility to create ions that can pass through the cell membrane, causing several reactions inside the cell. Cr(VI) penetrates the cell *via* the sulphate transport system. When passing through the cell membrane, an immediate reduction process occurs, where the chromates are broken down into different intermediates, such as the unstable and reactive forms Cr(V), Cr(IV) and reactive oxygen species (ROS). In addition to already existing cellular reductants in the cell such as ascorbic acid, flavoenzymes including cytochrome P-450, and glutathione, Cr(V) and Cr(IV) further degrade to the stable form Cr(III). The reduction of the intermediates contributes to protein and DNA damages and the ROS production has the possibility to interact with DNA complexes and cause oxidative stress, inflammation and cell proliferation. The mechanism of Cr(VI) toxicity can be seen in Figure 2.4. Lately, recent studies have shown a biological relevance of nonoxidative mechanisms in Cr(VI) carcinogenesis, allowing even more mechanisms of Cr(VI) toxicity. (Mishara & Bharagava, 2016)
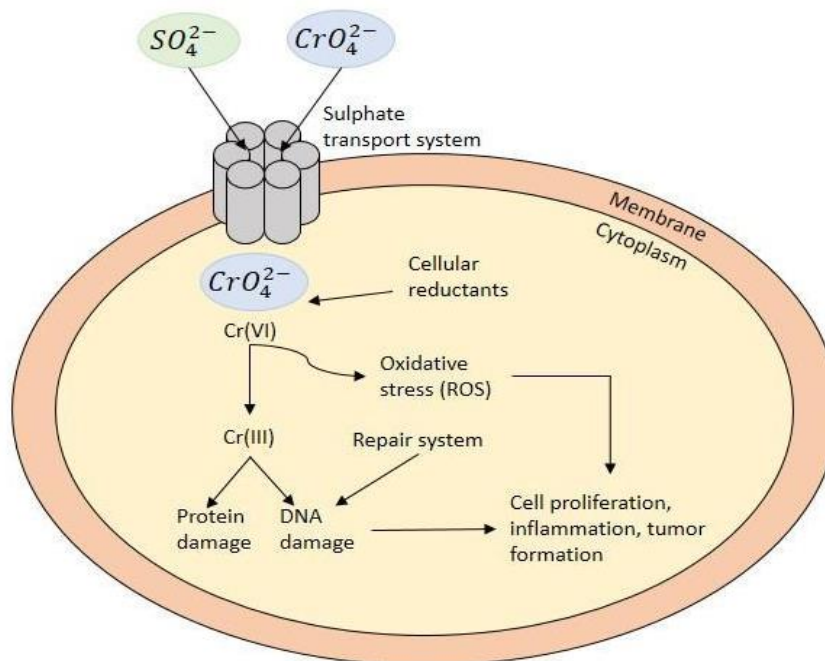
Figure 2.4: *An illustration of how Cr(IV) influences a human cell. Chromates pass through the cell membrane via the sulphate transport system. A series of reactions are started where the chromates are degraded to its final form Cr (III). Through the process, free radicals are released causing the cell oxidative stress, cell proliferation, tumor formation, DNA damages, etc.*
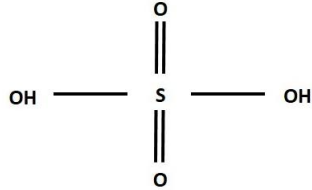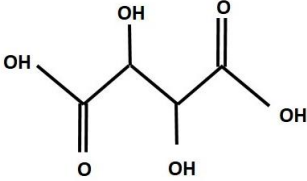
2.8.1 Replacements of hexavalent chromium in the aircraft industry

Due to Cr(VI) toxicity, it has been vital to find Cr-free electrolytes that can replace Cr-based surface treatments. Since it is important that the electrolyte contributes to the formation of a porous anode film on the substrate, an electrolyte that meets the requirements for the aluminum oxide fabrication is required. Therefore, acidic electrolytes are preferred. Acidic electrolytes are divided into three groups depending on their structure: inorganic acids, organic carboxylic acids, and organic cyclic acids. Chromic acid is classified as an inorganic acid which makes it favorable to replace it with an acid with similar structure and properties, such as sulphuric acid. (Kikuchi *et al.*, 2015)

Sulphuric acid is classified as an inorganic acid and is a favored substitute to chromic acid for several reasons. It has the capacity to anodize effectively at low voltages (15-40 V), create a porous oxide film with a pore diameter less than 100 nm, improve the mechanical properties of the substrates when anodizing at low temperatures ($\leq$ 0 °C), and has a low purchase price (Kikuchi *et al.*, 2015). Sulphuric acid can be used for anodizing, but commonly a modifier such as tartaric acid is added to provide even more advantages. Tartaric acid is classified as an organic carboxylic acid and contributes to a corrosion resistance comparable to chromic acid. The chemical structure of the sulphuric and tartaric acid can be seen in Table 2.4. During anodizing, tartrate ions interact with Al cations resulting in Al tartrate. During subsequent rinsing, the Al

tartrate produced can precipitate at the pore walls, which consequently contributes to a limited susceptibility to corrosion since the Al tartrate can act as a buffer and re-dissolve if exposed to a corrosive environment. Moreover, an electrolyte consisting of tartaric and sulphuric acid can reduce the anodizing process time (Museux and Theilmann, 2009) and the oxide growth rate, resulting in a thinner final film on the substrate than in normal sulphuric acid (Abrahami *et al.*, 2017).

Table 2.4. Schematic illustration of the chemical structure of the sulphuric acid and tartaric acid.

The usage of tartaric sulphuric acid (TSA) is not restricted like chromic acid. Neither tartaric nor sulphuric acid are carcinogenic, making them easier to handle in an anodization process. Also, they are more environmentally friendly since less energy is required due to the shortened anodizing process time (Museux and Theilmann, 2009) and the capacity to anodize at low temperatures and voltages (Kikuchi *et al*., 2015). Based on the stated advantages, it can be concluded that TSA may act as a good substitute for Cr-based surface treatments. Recently, Saab AB adapted TSA to its processes and in order to follow the Saab AB standard, TSA will be used for this project as well.

2.9 Powder coating

Another common surface treatment of Al alloys to improve protection of corrosion in the automotive and aerospace industry is paint coatings. Unfortunately, most of the paints used in these industries contain hexavalent chromium as well as organic solvents (Vargel, 2004; Valdesueiro *et al*., 2017). Some of these solvents contribute to adverse health effects and air pollution as volatile organic compounds (VOCs), when emitted during the painting operation. VOCs are a precursor of ozone and have the ability to form ground-level ozone through photochemical reactions with the traffic-related pollutant nitrogen oxide (NOx) (Epa and OAR, 2014; Kim, 2011). Despite the fact that ozone in the stratosphere (upper-level) plays a protective role against UV-light, ozone at ground levels is a harmful air pollutant that have a severe impact on the photosynthesis and thereby contributes to negative effects on vegetation and ecosystems (Manisalidis *et al.,* 2020).

Consequently, there exists regulations and directives in Sweden, also known as the paints directives, to limit the emissions of substances, such as VOCs, that promotes the formation of

ground-level ozone (Swedish Chemical Agency, n.d). Therefore, the aircraft industry needs to find substitutes with similar characteristics as for the wet-paint coatings and in recent years powder coating has been developed in order to reduce the solvent contents in paints (Kim, 2011).

Powder coating is a powder-based coating technique with several advantages compared to liquid-based paints. One crucial advantage is that the powder coating is more environmentally friendly since they do not contain organic solvents (Valdesueiro *et al.*, 2017). Other advantages are that powder coating is a method considered more resistant to corrosion, chemicals and weather than conventional solvent-based paint coatings (Sharifi *et al.*, 2017) and that minimal waste is produced when applied due to the applying technique (Maldonado et al., 2009).

The applying technique means that the powder coating agent is being charged and sprayed onto an electrified surface, making the charged particles adhere firmly to the object. Further, the powder is melted and cured in an oven, which results in a hard-continuous coating. By using powder coating it is easy to achieve a smooth surface, which is a desirable property for the aerospace industry (Manufacturing Guide Sweden AB, n.d.).

2.9.1 Powder coating for conventional and AM Al alloys

In a study conducted by Maldonado et al. (2009), powder coating was performed for the Al alloy 2024-T3. The alloy underwent different curing temperatures and hardness, strength, and conductivity were evaluated. The results indicated a successful powder coating, in both high and low curing temperatures, for industrial use. The powder particles adhere well, but the mechanical properties were negatively affected when cured at high temperature (Maldonado *et al.*, 2009). Other conclusions for Al alloy 2024-T3 have not been registered in literature since this application is very new and still under investigation for the aircraft industry. A similar scenario is there for the AM alloys where very little or no literature showing trials with powder coating exists, which makes this project even more exciting. The results given will provide a deeper understanding of powder coating on both conventional and AM alloys. It can be speculated that the rougher surface of AM alloys compared to the conventionally produced alloys will prove for different surface treatment properties and furthermore, other adhesion properties.

2.9.2 Adhesion properties

In order to succeed with powder coating, it is important that Al alloys prove for adhesion. Adhesion can be explained as an attraction between two dissimilar phases and can be divided into several classes due to the reason of attraction, such as mechanical adhesion, chemical adhesion and electrostatic adhesion. The bonding strengths of adhesion depends on the type of attraction. (Laurén, n.d.)

The adhesion properties are affected by parameters such as the materials morphology and its wettability. As mentioned earlier, anodization is performed to improve adhesion properties for

the metal (Vargel, 2004). According to a study conducted by Guo et al. (2013), the adhesion properties are dependent on the porous structure of the formed oxide layer during anodizing since it affects the morphology of the metal. For good adhesion, it is of importance that the coating spreads out of the surface since a good spreading contributes to a good penetration of the coating into the surface. The spreading properties are closely related to the morphology of the material (Laurén, n.d.). In order to understand one material's spreading properties, it is of interest to characterize materials wettability. In this project, this will be done by investigating the contact angle of a droplet which further will be explained in the characterization section below.

3 | Characterization methods

In this section, the theories of the methods used to identify the characteristic of the sample are described. Firstly, profilometry will be performed to study the Al alloys roughness and their Ra- and Rz-values. Secondly, light microscopy will be applied to study the surface of the alloys. Thirdly, contact angle goniometry will be performed to evaluate the wettability of the sample. At last, scanning electron microscopy and ImageJ will be used to investigate the morphology of the anodic coating.

3.1 Profilometry

To determine a surface topography, a profilometer can be used. It is an instrument that is easy to handle and in short time calculates different parameters that indicates a surface texture and curves. In this thesis a stylus profilometer is used.

A stylus profilometer consists of a needle, a handheld computer and an arm that links these pieces together. The needle is applied onto the surface for the purpose of physically sensing the structure of the surface in all directions - X, Y and Z. Even though the needle is sensitive, there are some issues with the instrument. When crossing the surface some of the depth may be too narrow, making it difficult for the tip to reach the bottom. Thereby, the measured profile may not fit the actual profile (Optical Profilometry - Nanoscience Instruments, n.d.). A clarified illustration of the instrument can be seen in Figure 3.1.
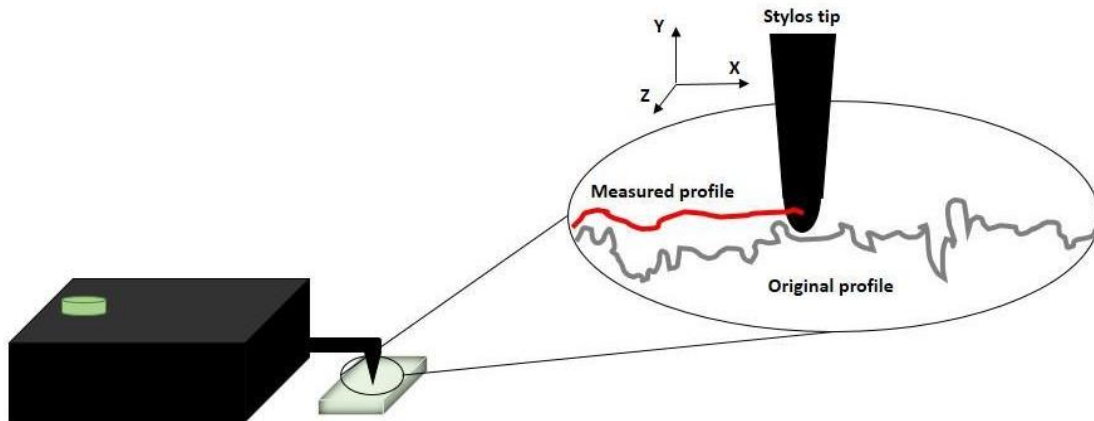
Figure 3.1: An illustration of a stylus profilometer. The instrument consists of a needle, a handheld computer and an arm that links the pieces together.

Basic surface texture parameters and curves are given from a profilometer measurement, such as *Ra* and *Rz*. *Ra* is an amplitude average parameter showing an arithmetical mean deviation, *Z(x)*, of ordinate values within a sampling length, *L*. *Rz* is an amplitude parameter showing the maximum height of the profile - a summary of the highest peak, *Rp*, and the largest depth, *Rv*,

within a sampling length. Ra and Rz are calculated according to Equation 3.1 and 3.2 (Accretech Tokyo Seimitsu, n.d.):

$$Ra = \frac{1}{L}\int_0^L |Z(x)|dx \qquad \text{Eq. (3.1)}$$
$$Rz = Rp + Rv \qquad \text{Eq. (3.2)}$$

The values of the surface roughness could vary, depending on the measurement method used and the orientation of the surface. The values stated in Table 3.1, give an indication of what values that can be achieved for certain surfaces. (apworks, n.d.; EOS M 290, n.d.)

Table 3.1. *Ra- and Rz-values for the AlSi10Mg and Scalmalloy$^{®}$ according to the manufactures.*

Al alloy	Ra [μm]	Rz [μm]
AlSi10Mg (EOS M 290, n.d.)	6 - 10	30 - 40
Scalmalloy$^{®}$ (apworks, n.d.)	10	80

3.2 Light microscopy

In order to characterize the alloy surface's, a handheld light microscope can be used. A handheld light microscope is connected to an USB contact, making it possible to connect the microscope to a computer equipped with proper software. The microscope is equipped with several sizes of nozzles which makes it possible to adjust the magnification. A shorter nozzle contributes to a larger magnification and vice versa. To create sharpness, the microscope is equipped with a magnification tool. The instrument is equipped with a digital camera that can take pictures of the studied surface which further can be saved on the computer used at the time. (DinoCapture User Guides, n.d.)

3.3 Contact Angle Goniometry

Contact angle (CA) goniometry is a method used for measuring surface wettability. In order to carry out goniometry one can use the sessile drop method, a method based on placing a liquid droplet on a surface by a syringe. The droplet is detected by a camera that is connected to a computer where software calculates an angle between the droplet (liquid phase) and the surface of the Al alloy (solid phase) (Makkonen, 2016). An illustration of a common set-up can be seen in Figure 3.2.
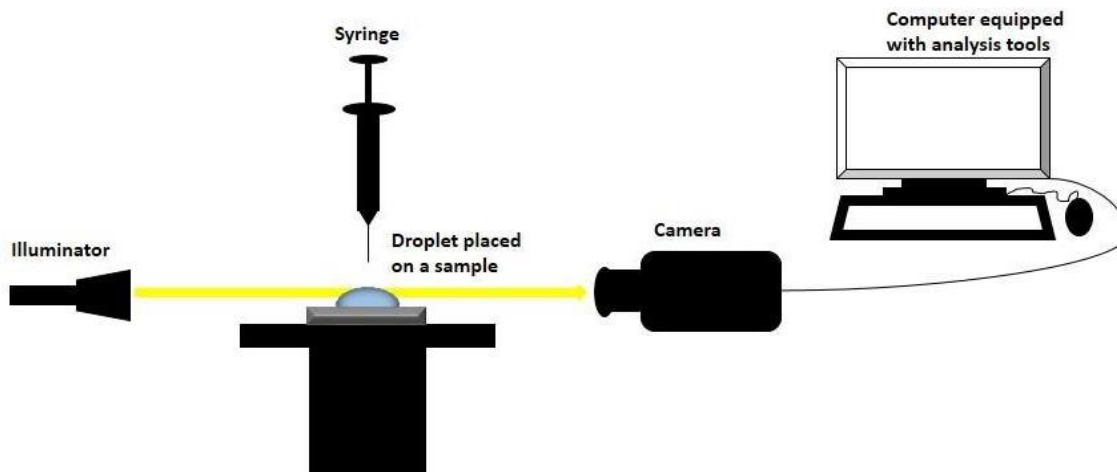
Figure 3.2: A set-up of contact angle goniometry consisting of an illuminator, a syringe, a horizontal table for the substrate and a computer with a proper software.

When placing a droplet on a substrate, three different tensions between the three different phases - liquid, solid and gas, occur according to Figure 3.3. The forces between molecules within the droplet - cohesive forces, and the liquid and the solid phase - adhesive forces, form an angle further referred to as the contact angle, θ. Depending on the wettability of the surface, θ can vary from very small values to high. High values ($\theta > 90$) indicate a hydrophobic substrate due to the weak adhesive forces, and low values ($\theta < 90$) indicate a hydrophilic substrate due to stronger adhesive forces. When $\theta = 0$ the surface is referred to as completely wettable (Barnes & Gentle, 2005). The symmetry of a droplet may vary; therefore, CA is measured on both sides of a droplet, i.e. θ_{left} and θ_{right}, which further makes it possible to calculate an average of CA to reduce uncertainty.
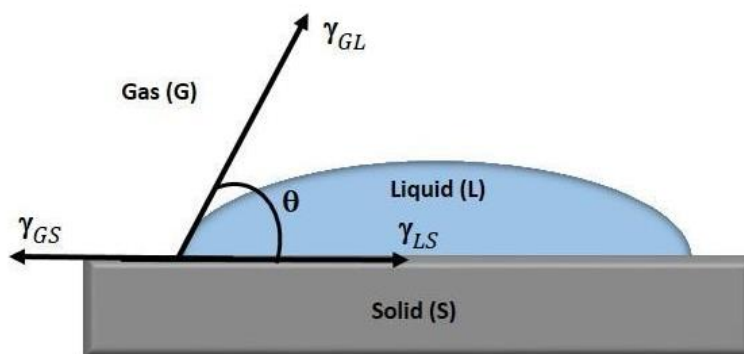
Figure 3.3: An illustration of the interfacial tensions acting on the three phases where θ describes the contact angle. γ_{GS} describes the tension between the gas phase and solid face. γ_{GL} describes the tension between the gas phase and the liquid phase and γ_{LS} describes the tension between the solid phase and the liquid phase.

The CA in Figure 3.3 is described by Young's equation. Although Young's equation is understood by the balance between the three forces, it also has an origin in minimizing the free energies of the system. However, the scalar of the thermodynamic surface energies is often misunderstood when arguing about the surface wettability making it easier referring the

wettability to the CA of the three interfacial tensions. The idea of balanced interfacial tensions results in the following equation, Eq. (3.3) (Makkonen, 2016):

$$\gamma_{SG} = \gamma_{LS} + \gamma_{GL} \cdot cos\theta \qquad \text{Eq. (3.3)}$$

The equation relies on ideal surfaces (Makkonen, 2016). On uneven surfaces the liquid droplet has the ability to either penetrate the irregularity or to stay on top of it, making Young's equation insufficient for detecting wettability and CA for rough surfaces. Consequently, the Young model needs to be supplemented with the Wenzel or Cassie-Baxter model in order to obtain a correct CA and properly understand a surface's wettability.

The Wenzel model describes the CA (θ_h) for a liquid droplet that penetrates the irregularities, shown in Figure 3.4, and is described by the equation, Eq. (3.4), where r indicates the ratio of the actual surface against the apparent surface (roughness factor) and θ is CA of an even surface. (Tabar *et al.*, 2019)

$$cos\theta_h = r \cdot cos\theta \qquad \text{Eq. (3.4)}$$

In those cases, the liquid droplet does not penetrate the rough surface and creating air pockets according to Figure 3.4, the Cassie-Baxter model is needed. The Cassie-Baxter equation is described in Equation (3.5), where f indicates the contact area between the droplet and the substrate. (Tabar *et al.*, 2019)

$$cos\,\theta_h = f \cdot cos\,\theta_s - (1 - f) \qquad \text{Eq. (3.5)}$$

According to the Wenzel and Cassie-Baxter model, a solid's wettability can be described as: an increased CA with an increased roughness indicates a hydrophobic surface and a reduced CA with an increased roughness indicates a hydrophilic surface. (Lin *et al.*, 2018)

As for this thesis, samples with both rough and smooth surfaces will be measured resulting in all three models being relevant when discussing the wettability. Contact angle goniometry will be used as a first evaluation of the anodic and powder coating.
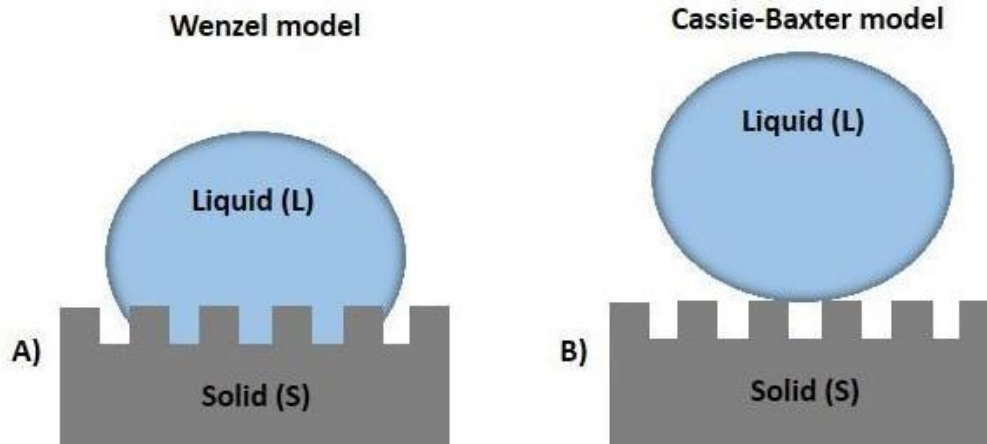
Figure 3.4: *A) An illustration of the Wenzel model. B) An illustration of the Cassie-Baxter model.*

3.4 Scanning Electron Microscopy

Scanning electron microscopy (SEM) is an imaging technique used to deeply detect morphologies on surfaces. This technique uses a primary electron beam with a raster pattern for scanning the object and generates high-resolution images of a surface's structure. The resolution of the image largely depends on the wavelength. (Stokes, 2008)

The electrons interact with the atoms on the object, which in turn sends back backscattered electrons (BSEs), secondary electrons (SEs), photons and characteristic X-ray. Those that are emitted can be collected and further be used to form an image. In SEM, the secondary electrons and backscattered electrons signals are registered respectively to give knowledge about the object's topography and composition. Since the surface has an impact on the generated signals, different objects and structures can be distinguished from each other. (Stokes, 2008). An overview of the useful signals that are generated when the primary electron beam strikes the surface is illustrated in Figure 3.5.
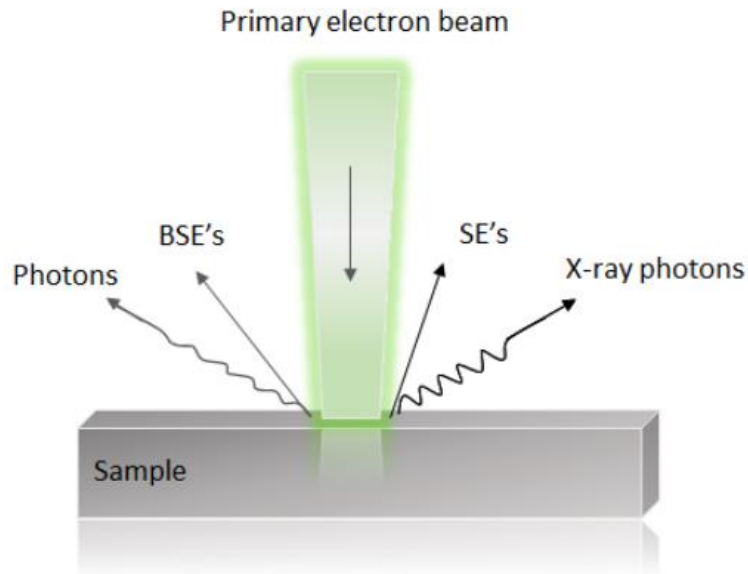
Figure 3.5: *An overview of the principle of SEM. The primary electron beam penetrates the sample and interacts with the samples' electrons. The interaction generates secondary electrons (SE's), backscattered electrons (BE's), photons and X-ray photons.*

The backscattered electrons are originated from elastic collisions between the surface's atoms and the electron beam. The collision with an atom in the interaction volume of the sample, results in a change in the electrons' trajectory and the electrons are thereby backscattered. The amount of BSE's depends on the atomic number Z and therefore depends on the chemical composition of the sample surface. This results in the BSE's being useful for the determination of the sample composition. Secondary electrons are a result of an inelastic interaction between the electron beam and the surfaces' atoms. These electrons have lower energy compared to BSEs and are used for analyzing the topography of the sample. (Nanakoudis, 2019)

The SEM-system consists of several components and is illustrated in Figure 3.6. The sample surfaces of interest are placed in a chamber where they are fixed. The electron source is operated under vacuum to reduce contamination of the electrons and to achieve an improved electron scattering. The electron beam is produced by applying a high voltage to a filament such as a thermionic emitter or a field emission source. Electromagnetic lenses are used to focus and shape the primary electron beam. The detector system collects and processes the electron signals and is visualized on a display. (Stokes, 2008; Nanakoudis, 2019) In this master thesis, SEM is used to create images over the anodized sample surfaces to visualize the morphology of the anodic coating for the AM samples.
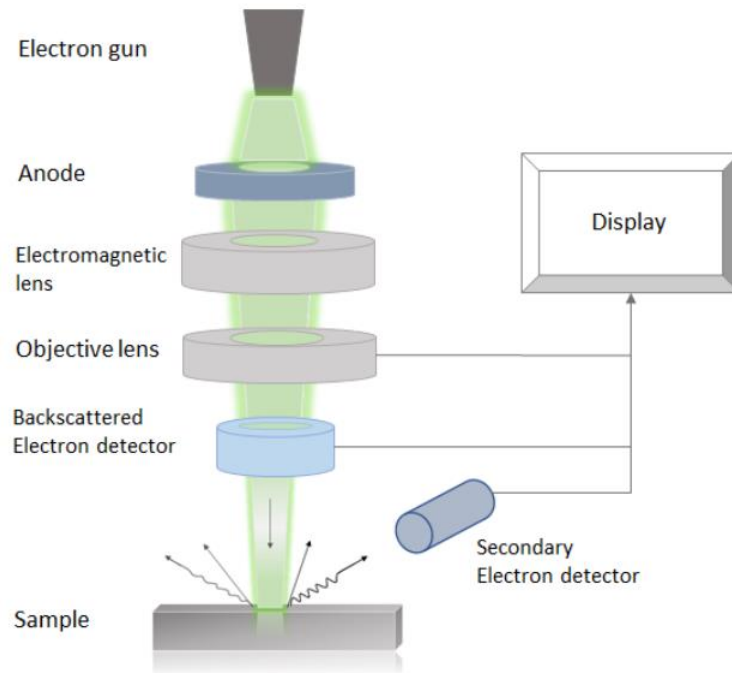
Figure 3.6: *An illustration of the Scanning Electron Microscope (SEM) set-up system. The microscope consists of an electron gun, an anode, an electromagnetic lens, an objective lens, a backscattered electron detector, a secondary electron detector and a computer.*

3.5 ImageJ

ImageJ is a free JAVA-based image-processing platform available for Windows, Mac OS X and Linux. It was developed in 1997 (ImageJ, n.d.) and has since then made it possible to develop low-cost image-processing (Barboriak et al., 2005). The software reads TIFF, PICT, PICS and MacPaint files, making it possible to investigate different kinds of image formats. ImageJ can be used to detect area mean, centroid, perimeter, etc. of a specific region in a picture. Thereby, ImageJ can be used to detect Al alloy´s morphology, including measurement of the pore diameter and interpore distance (Introduction ImageJ, n.d.).

4 | Experimental

The experimental work performed during this master thesis aims to investigate the properties of the anodic coating on additive manufactured Al alloys by studying morphology, porosity, and wettability of the oxide layers achieved by anodization. There will also be experimental work performed to investigate the behaviors of powder coating on three different Al alloys, one conventionally produced alloy and two AM alloys. There was also an interest in investigating if blasting will have any impact on the anodic and adhesion properties of AM alloys. Therefore, some of the AM metal samples undergo a blasting process at Saab AB. In this section, the materials and chemicals for the experiments, procedures and conditions are described. The workflow of the experiments was performed according to Figure 4.1.
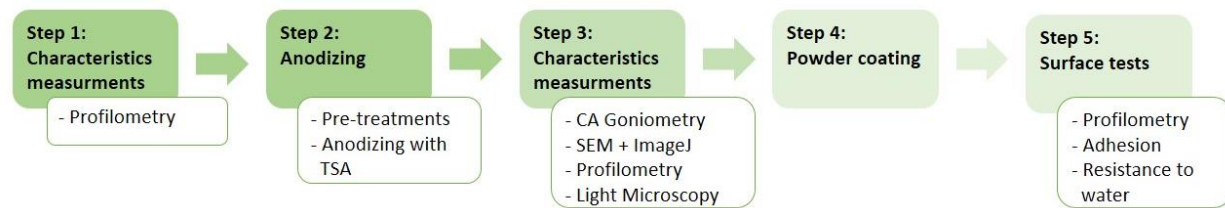
Figure 4.1: *An illustration of this master thesis experimental workflow.*

4.1 Materials

The anodization of the AM Al alloys was conducted at the Department of Physics, Chemistry and Biology at Linköping University. The instruments, materials and chemicals used in the experimental work during this thesis are shown in Table 4.1 and 4.2.

Table 4.1. *Materials and chemicals used in the different experiments during the master's thesis, their application and how they are acquired.*

Material & Chemicals	Application
Al Alloy samples: 2024-T3, Scalmalloy®, AlSi10Mg (raw and blasted)	Samples for anodization and powder coating.
Milli-Q water	Rinsing of samples, anodizing pretreatment. Liquid for CA, TL-1 washing procedure of goniometer needle.
Acetone ($(CH_3)_2CO$)	Degreasing of sample, anodizing pretreatment.
Alkaline degreasing solution	Alkaline degreasing, anodizing pretreatment.
Pickling solution	Pickling bath for rinsing of samples, anodization pretreatment.

Tartaric sulphuric acid	Used as anodizing electrolyte.
Hydrogen peroxide (25 % H_2O_2)	TL-1 washing procedure of goniometer needle.
Ammonia (25% $NH_3 \cdot H_2O$)	TL-1 washing procedure of goniometer needle.
Nitrogen gas (N_2)	Blow drying of samples and goniometer needle.
Powder coating (epoxy-based korroprimer)	Used in the powder coating process.

Table 4.2. *Instruments used in the different experiments during the master's thesis, their application and how they are acquired.*

Instruments	Application
Stylus profilometer	Measurements of the roughness of the samples.
CAM 200 Optical Contact Angle Meter	Measurements of CA on sample surfaces.
Zeiss LEO 1550 SEM	Characterization of sample surfaces.
Dino-Lite Digital Microscope	Characterization of sample surfaces.
Powder coating machine with electrostatic gun	Used to apply powder coating on the sample surfaces.

The samples of the Al alloy 2024-T3, AlSi10Mg and Scalmalloy® were used in this master's thesis and the size and shape of the samples are illustrated in Figure 4.2.
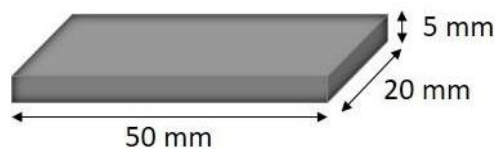
Figure 4.2: *A design of the sample size used in this master thesis.*

4.2 Methods

In this section, the different methods are described and illustrated. The anodizing process including the pretreatment steps is the most essential method. The wettability and morphology were measured by using contact angle goniometry and SEM. The surface roughness was measured by using a stylus profilometer. All methods were performed on both raw and blasted

sample surfaces. The blasted samples were blasted with Al oxide at a pressure of 4 Bar at Saab AB.

4.2.1 Characterization of the surface roughness

Before and after the anodizing process, measurements of the surface roughness on both raw and blasted samples were conducted by a profilometer provided by the department IEI - management and engineering, at LiU. The measurements were conducted using a stylus profilometer by placing the instrument on the surface of interest and measuring the same surface three times on the same sample. The profilometer calculates the values of Ra and Rz for the different Al Alloys. The given values from each measurement were compiled and an average value and standard deviation of Ra and Rz was calculated for each alloy.

4.2.2 Anodization

The anodization was conducted using the same set-ups used in the previous master's theses conducted during spring 2019 at LiU. The anodization process is one of the most fundamental processes of the experiments during this project and was conducted at IFM, LiU. An overview of the anodization process is illustrated in Figure 4.3, and all steps are thoroughly described in this section.
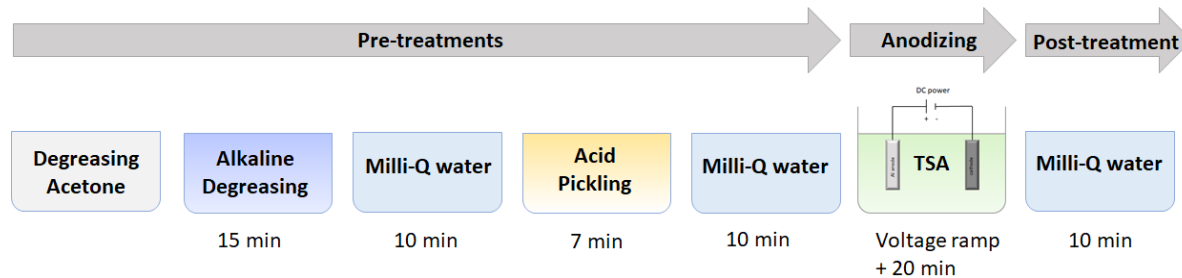
Figure 4.3: An overview of the anodizing process performed during the project. The three different Al alloys were pre-treated and were then anodized in TSA.

4.2.2.1 Pre-treatments

The following pretreatments were conducted according to Saab AB's standard. Before the alkaline degreasing bath, the surfaces were rinsed with Milli-Q water and acetone to remove grease and other contaminants. All the samples were immersed in an alkaline degreasing bath at 54-56 °C for 15 minutes while stirred by a magnetic stirrer. Thereafter the samples were rinsed again in an ultrapure Milli-Q water bath at room temperature for 10 minutes. This was followed by an acid pickling bath at room temperature for 7 minutes and thereafter the samples were rinsed and immersed in an ultrapure Milli-Q water bath at room temperature for 10 minutes.

4.2.2.2 Anodization process

An investigation of the anodizing process was done by performing the anodization according to Saab AB's standard. The metal samples were anodized in two procedures. One where the 3

different alloys were simultaneously anodized in the same bath, further referred to as procedure 1, and another where the alloys were anodized separately, further referred to as procedure 2. The anodizing process according to Saab AB's standard protocol was performed in the electrolyte TSA. According to the protocol the electrolyte temperature should be carried out at 39 °C. Due to the difficulty to control the temperature in this project, the temperature was obtained within the interval 38-41°C. The voltage was increased using a voltage ramp of 1.4 V every 30 s from 0 V up to 14 V. Thereafter, the voltage was kept at 14 V for 20 minutes. During the anodizing process, the current was observed with a multimeter. The electrolyte was during the whole process stirred with a magnetic stirrer. After the anodizing process, all Al alloy samples were rinsed and immersed in a Milli-Q water bath for 10 minutes.

4.2.2.3 Set-up

The set-up used in this master thesis was designed by the previous master thesis conducted by Poot (2019). This set-up was designed to allow a larger number of samples to be anodized at the same time. The set-up consisted of four glass boxes with plastic lids containing alkaline degreasing solution, pickling solution, TSA and Milli-Q water. The samples were tightly attached between two stainless steel plates with screws to improve the contact between the sample surfaces and the metal plates, hence improving the current flow from the DC power supply. Six surfaces could be anodized simultaneously.

The cathode was U-shaped and made of stainless steel and was attached to the plastic lid. The cathode had the dimensions $150 \times 80 \times 90$ mm. Two screws, one attached with the anode and the other one with the cathode, served as connection points for the DC power supply. A picture of the used set-up is shown in Figure 4.4 below.

Figure 4.4: *A picture over the used set-up. The set-up contains a thermometer, a heating plate, a bath, a DC-power and a multimeter.*

4.2.3 Light microscopy

Light microscopy was performed by using Dino-Lite Digital Microscope. Before performing measurements, a new calibration profile was created for the microscope, by using the calibration target. The microscopy was then placed on top of the surfaces and pictures of the samples were taken before and after anodization. The shortest nozzle, N3C-E, was used to get the largest magnification possible, approximately up to 200 ×. The pictures were saved on the computer used at the time which were equipped with the software DinoCapture 2.0. The magnification of the obtained pictures reached 180x.

4.2.4 Contact Angle Goniometry

After the anodizing process, goniometry was performed. In this thesis a Cam 200 optical Contact Angle Meter, KSV Instruments LTD was used for measuring CA and can be seen in Figure 4.5. Goniometry was conducted at LiU and was divided into two major steps - pretreatment and contact angle measurement. The pre-treatment involved a washing procedure to ensure good cleanliness during contact angle goniometry, further referred to as TL-1 wash. The needle was carefully taken off the syringe by a pair of tweezers and put in a cup filled with Milli-Q water,

ammonia and hydrogen peroxide. The solution relationship was set to 1:1:5. Tweezers were placed in another beaker filled with the same washing solution. The beaker with its contents was separately heated to 85°C, washed with Milli-Q water and blow-dried with N_2. The tweezers were heated for 10 minutes while the syringe needle was heated for 2-3 minutes. After the TL-1 wash, the needle was carefully attached to the syringe and attached to the instrument again.
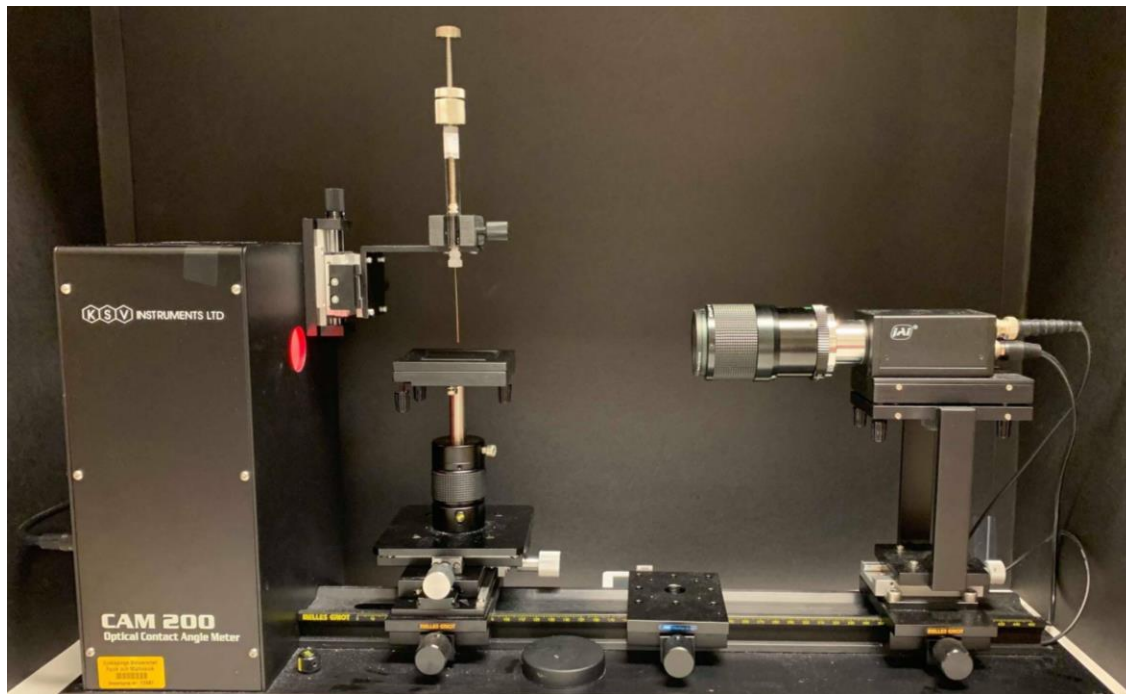
Figure 4.5: *The contact angle goniometry used at LiU.*

In step two CA was measured by using the sessile drop technique. The sample to be examined was placed under the needle and the settings of the instrument were adjusted to get a clear view. A droplet was carefully placed onto the sample surface and photographed. The software complement KSV Contact Angle Measurement system was used to calculate CA, left and right angle, from the taken picture. In most cases, there were difficulties finding the baseline. For those measurements, the baseline was set manually. When CA was below 10 degrees, the software instrument could not detect an angle and the value was set to Non-detectable (N/D). For each sample, at least three droplets were tested and calculated.

4.2.5 Scanning Electron Microscopy and ImageJ

SEM was performed at LiU by using a secondary-electron imaging mode called Zeiss LEO 1550 SEM with one GEMINI column. To succeed with the measurement, a pretreatment in the form of a sputtering was performed by using the instrument Leica EM SCD 500. The substrates were coated in copper tape and sputtered with platinum (Pt) in order to improve conductivity. Normally, it is possible to sputter and measure eight samples at the time. However, for this project, two samples were investigated at the same time due to the large size of the samples.

During the SEM measurement, the sample's surfaces were scanned and pictured at different positions and magnifications. The magnification varied among the samples but was set from 25kx up to 300 kx. The SEM images were later analyzed by the ImageJ software for knowing the morphology of the samples. Pore diameter, interpore distance, pore wall thickness and porosity were measured and calculated by setting a scale based on a known distance. Several measurements were made for each purpose and the given values from each measurement were compiled and an average value and standard deviation were calculated.

4.2.6 Powder coating

The samples that did not undergo SEM were prepared for powder coating. In total, 12 samples were prepared for powder coating and the samples were blasted on one side and raw on the other. The pretreatment for each alloy can be seen in Table 4.3. The anodization was performed at LiU and is previously described in section 4.2.2. The primer used contained solvents and was applied at Saab AB's production according to the Saab AB standard. The primer is used to improve the adhesion properties.

Table 4.3. Table showing the number of samples that were prepared with different pretreatments before undergoing the powder coating process.

Pretreatment	2024-T3	Scalmalloy$^{\circledR}$	AlSi10Mg
Not anodized	1 (reference)	1	1
Anodized	1	1	1
Anodized + primer	1	1	1

The pretreated pieces were fixed in an Al wire which was hung on to a grounded rod in a fume hood. The samples were powder coated with a korroprimer two times on each side. The powdered samples were put in an oven for curing at a temperature of 125 ℃ for 40 minutes. Further, the thickness of the cured powder was measured for the reference material Al alloy 2024-T3.

Tests to control the success of powder coating were performed for all samples shown in Table 4.3. At first, a regular adhesion test was performed. The adhesion test means that a piece of adhesive tape is fastened firmly to the surface followed by quick removal. For a successful result, no traces of coating should be visible on the tape or removed from the sample according to Saab AB's standard. Secondly, the samples were put in a cup filled with water and placed in room temperature for 24 hours, air dried, and then exposed for an adhesion test again. Lastly, the samples were executed for a four-day long water bath at 40 ℃ before the last adhesion tests were conducted. The four-day long wet adhesion test was conducted by Element Materials Technology (EMT).

5 | Results

This master's thesis aim was to investigate the properties of the anodic coating on AM Al alloys by studying the morphology and wettability of anodic coatings achieved by anodization. Furthermore, the adhesion properties for powder coating were investigated. Herein, the results from the experiments are presented.

5.1 Anodization of untreated samples

As a first screening method, the color of the anodized samples were observed by visual inspection. When anodization was performed according to procedure 1, where the samples were anodized together, a color change could be obtained from the AlSi10Mg and Scalmalloy® alloy. In Figures 5.1 and 5.2, the colors of each sample before and after anodizing can be observed.
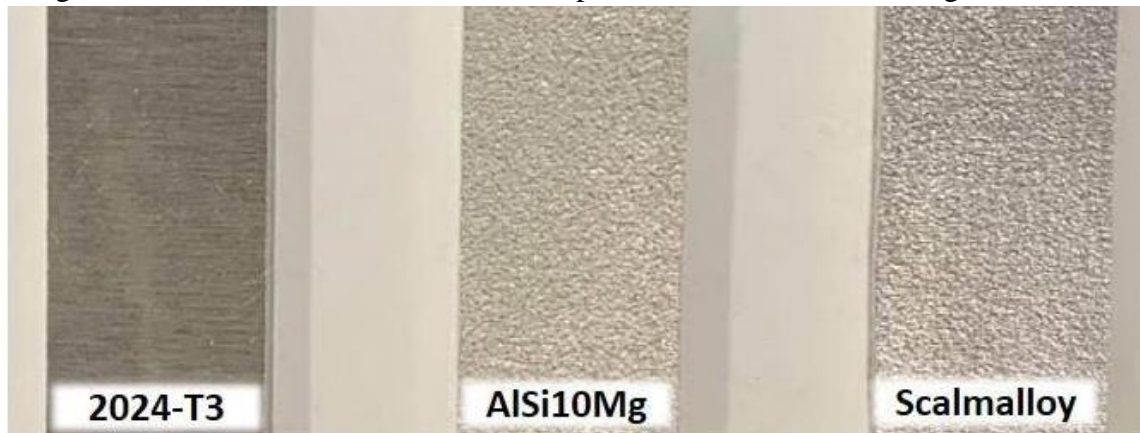
Figure 5.1: An image of the samples before anodization. From left to right: Al alloy 2024-T3, AlSi10Mg and Scalmalloy®.
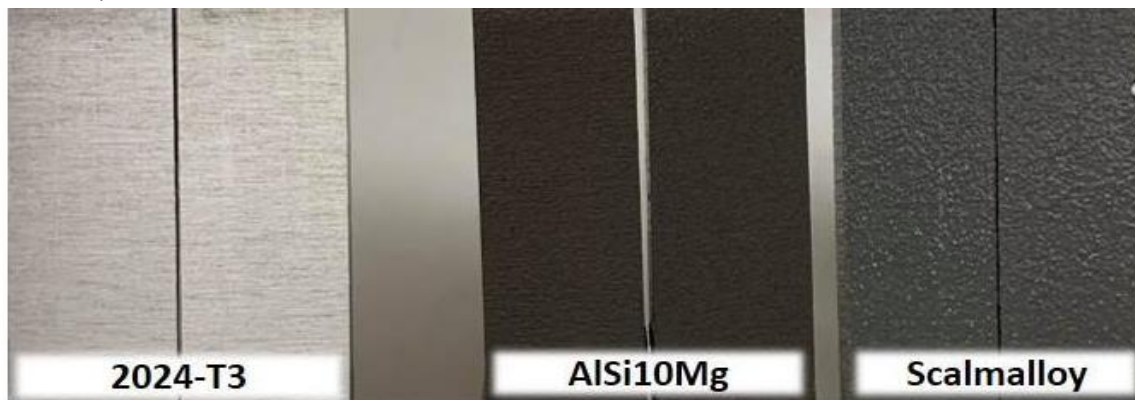
Figure 5.2: An image of the samples after anodization of six samples, according to procedure 1, two of each alloy. From left to right: Al alloy 2024-T3, AlSi10Mg and Scalmalloy®.

5.1.1 Current measurements

Three samples were anodized separately according to procedure 2 in order to observe and measure the electrical current for each alloy at a constant voltage of 14V. The current was observed at specific times [min] and measured in Ampere [A]. The results given were compiled and plotted and can be seen in Figure 5.3 below.
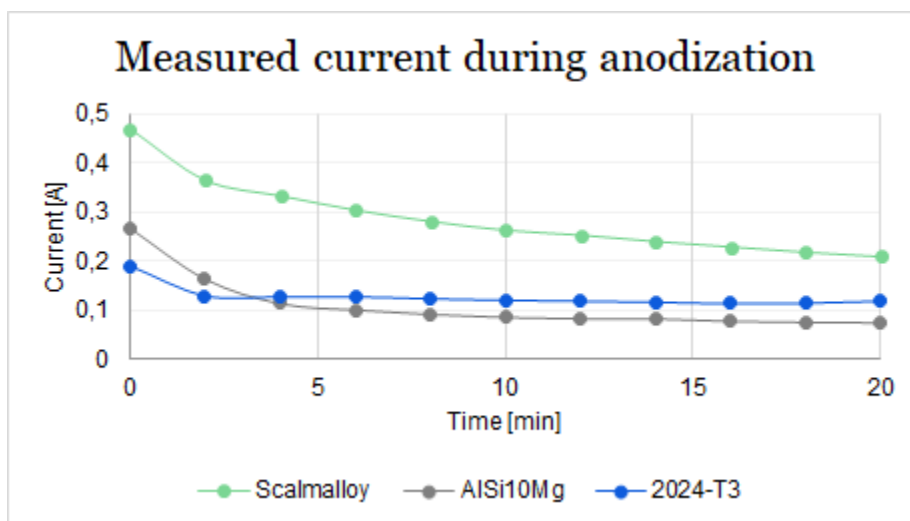
Figure 5.3: Showing the measured current during anodization. The dots in the figure are the time when the current was observed. To identify trends the dots have been linked together with drawn lines. The green line describes the current for Scalmalloy$^{®}$. The grey line describes the current for AlSi10Mg and the blue line describes the current for Al alloy 2024-T3.

5.2 Surface characterization

The morphology of the anodic coating and the adhesion properties were analyzed using light microscope, CAM and SEM.

5.2.1 Light Microscopy

The anodization was done according to procedure 1 in the same conditions as described above in the experimental section for all alloys. The images shown in Figure 5.4, were conducted by Dino-Lite Digital Microscope and were taken before and after anodization in order to get a first indication of changes on the surfaces. The upper images, A1, B1 and C1, in Figure 5.4 shows the surface sample of the reference material Al alloy 2024-T3, Scalmalloy$^{®}$ and AlSi10Mg before any pretreatments or anodization were performed, and the lower images shows the surface sample after pretreatments and anodization.
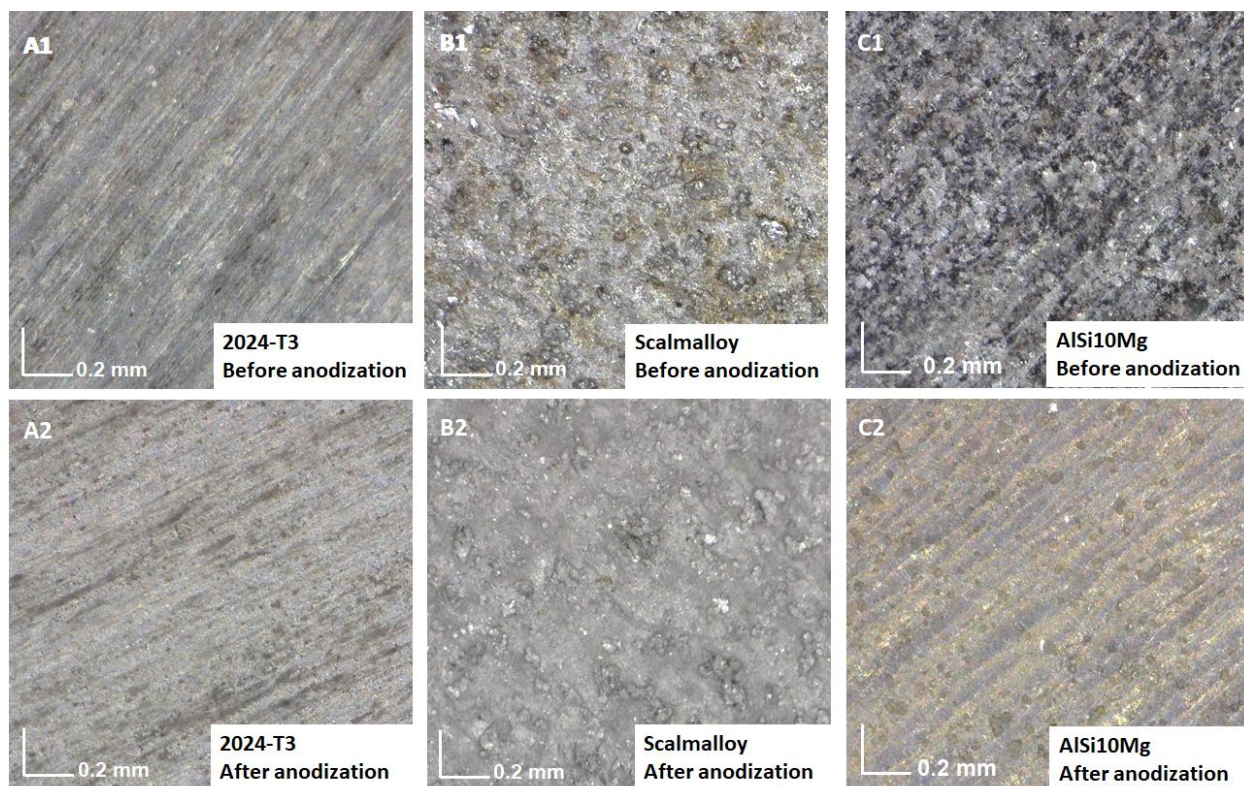
Figure 5.4: *Dino-Lite Digital Microscope image with the magnification 180 ×. A1) Microscope image of 2024-T3 before undergoing any pretreatments and anodization. A2) Microscope image of 2024-T3 after anodization. B1) Scalmalloy® before undergoing any pretreatments or anodization. B2) Scalmalloy® after anodization. C1) AlSi10Mg before undergoing any pretreatments or anodization. C2) AlSi10Mg after anodization.*

5.2.2 Wettability

Contact angle goniometry was performed in several areas of the surface, directly after the anodization. The images given from all the samples were compared and evaluated. In the figures below, Figure 5.5-5.7, a selection has been made according to the pictures which in a most representative way shows the wettability of the samples. Next to the pictures, the calculated CA and standard deviation from each measurement are shown.

Sample	CA [o]
2024 - T3	52.1 +/- *11.5*
Scalmalloy®	N/D (<10, A droplet is identified, no baseline identified)
AlSi10Mg	49.0 +/- *11.4*

36
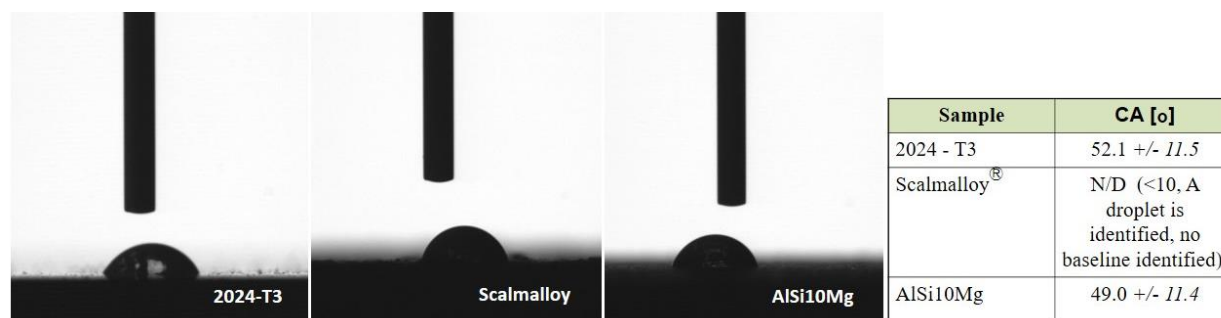
Figure 5.5: Shows the nature of a droplet on unmodified surfaces. As for Al alloy 2024-T3 the black spots on the surface indicate impurities. The CA was calculated for 2024-T3 and AlSi10Mg. As for Scalmalloy® a droplet was identified but the software was not able to perform a CA-calculation.

Sample	CA [o]
2024 - T3	12.2+/- 6.5
Scalmalloy®	0
AlSi10Mg	< 10
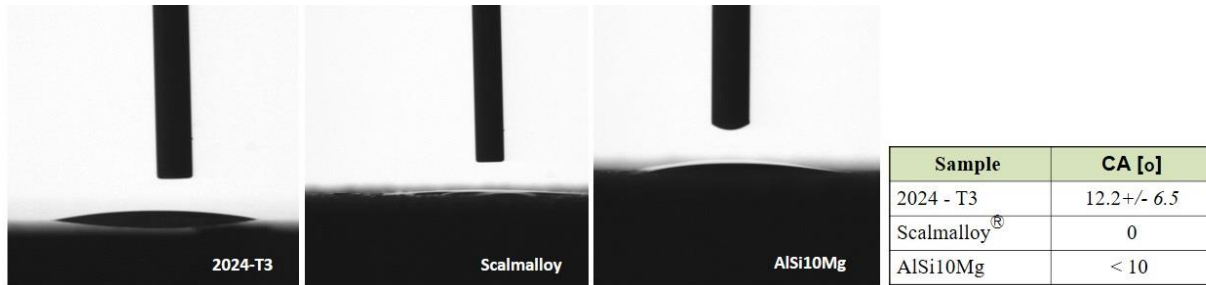
Figure 5.6: Shows the nature of a droplet on pickled alloys. For all Al alloys, the droplet has spread to different degrees on the surface. In the case of Al alloy 2024-T3 and AlSi10Mg, a droplet can be identified, and a CA could be calculated. In the case of Scalmalloy®, a droplet cannot be identified, and the CA could not be calculated.

Sample	CA [o]
2024 - T3	9.3 +/- 2.8
Scalmalloy®	0
AlSi10Mg	< 10
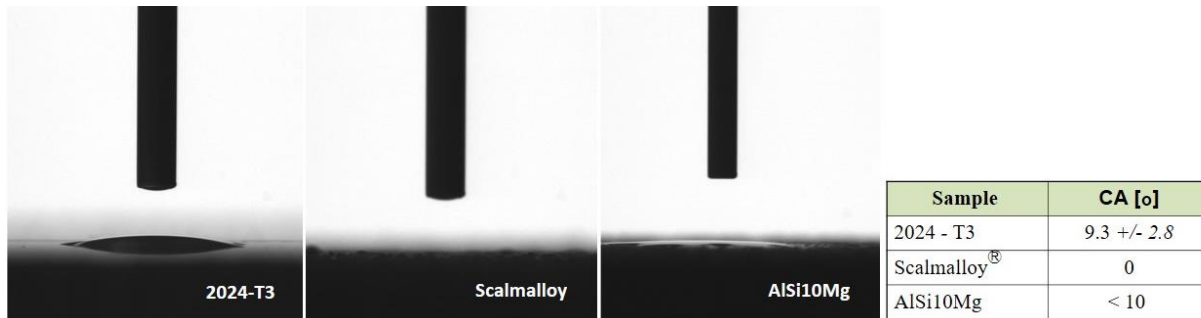
Figure 5.7: Shows the nature of a droplet on anodized Al alloys according to procedure 1 and Saab AB's standard. For all Al alloys, the droplet has spread to different degrees on the surface. In the case of Al alloy 2024-T3 and AlSi10Mg, a droplet can be identified, and a CA could be calculated. In the case of Scalmalloy®, a droplet cannot be identified, and the CA could not be calculated.

5.2.3 Morphology of three different alloys

The anodized alloys were investigated by using SEM. The pore morphology of the different surfaces was investigated at several magnifications and the results are shown in Figure 5.8. The alloys from left to right: Al alloy 2024-T3, Scalmalloy® and AlSi10Mg and the magnification from the top to the bottom: 25kx, 120kx and 300kx. For the smaller magnification (Figure 5.8, A1-C1), the surface structure was investigated. For the larger magnification (Figure 5.8, A2-C2, A3-C3), the pore morphology of the anodic coating was observed and studied. A porous structure was identified for all the sample surfaces.
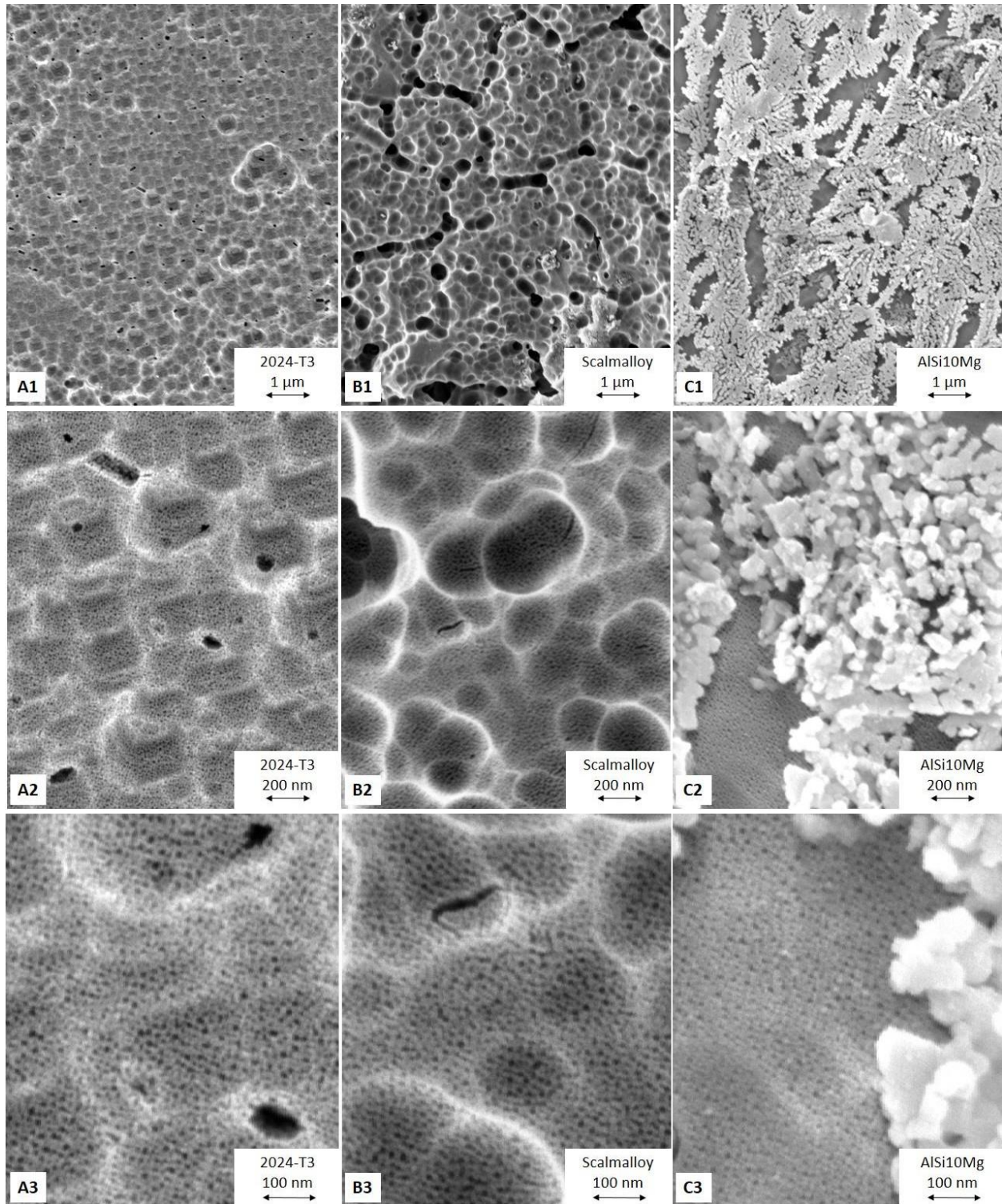
Figure 5.8: *Images received from SEM, where A=Al alloy 2024-T3, B=Scalmalloy$^{®}$, C=AlSi10Mg, 1=magnification 25 000x, 2=magnification 120 000x and 3=magnification 300 000x.*

From the SEM images, the pore morphology for the different surfaces were studied by using the software ImageJ. Pore diameter, interpore distance, pore wall thickness and porosity were

measured and calculated. The results from ImageJ are presented in Table 5.1. The pore diameter is highest for Al alloy 2024-T3 and the lowest for AlSi10Mg. The pore wall thickness is smallest for Al alloy 2024-T3 and highest for AlSi10Mg.

Table 5.1. *Shows the values for the pore diameter, interpore distance, pore wall thickness and porosity of each alloy.*

Sample	Pore diameter [nm]	Interpore distance [nm]	Pore wall thickness [nm]	Porosity [%]
2024-T3	9.2 ± *1.3*	22.5 ± *3.1*	7.2 ± *1.7*	31.9 ± *3.3*
Scalmalloy®	8.7 ± *0.9*	16.6 ± *3.6*	8.5 ± *3.6*	21.3 ± *2.6*
AlSi10Mg	7.6 ± *1.1*	22.5 ± *4.4*	17.1 ± *5.3*	11.1 ± *1.1*

5.3 Powder coating

When powder coating was performed, the powder thickness of the powder coating applied on Al alloy 2024-T3 was measured. The powder thickness was not measured for Scalmalloy® and AlSi10Mg since a reference value for those alloys do not exist. The thickness of powder coating for raw Al alloy 2024-T3 was measured to 41μm.

In this master thesis, three different tests in order to control the adhesion of powder coating to the substrate were performed. From the first adhesion test, where the samples had not been in a water bath, no differences could be obtained. All samples from Table 4.3 passed the test due to no powder coating being released. From the adhesion test performed after a 24h long incubation in water at RT, the powder coating was removed from one sample - raw Al alloy 2024-T3, which is illustrated in Figure 5.10. According to the coating removal, the raw Al alloy 2024-T3 was excluded from the last test. From the last test, where the samples were exposed to water for 4 days at 40°C followed by adhesion test, no difference could be obtained. The samples did not prove for impaired adhesion properties. A table of all powder coated samples after the adhesion tests can be seen in Appendix VII.

Figure 5.10: *All 9 samples after powder coating and all adhesion tests. Samples marked with green dots: unanodized samples with powder coating. Samples marked with red dots: anodized samples with powder coating. Samples marked with black dots: anodized + primed samples with powder coating. In each figure, the alloys from left to right is Al alloy 2024-T3, Scalmalloy® and AlSi10Mg.*

5.4 Profilometry

The results from each measurement have been used to calculate an average value for each alloy. A standard deviation for all the measurements for each alloy was also calculated. Profilometry was conducted before and after anodization, primer and powder coating, and the results from the profilometry are shown in Figure 5.11 and 5.12.
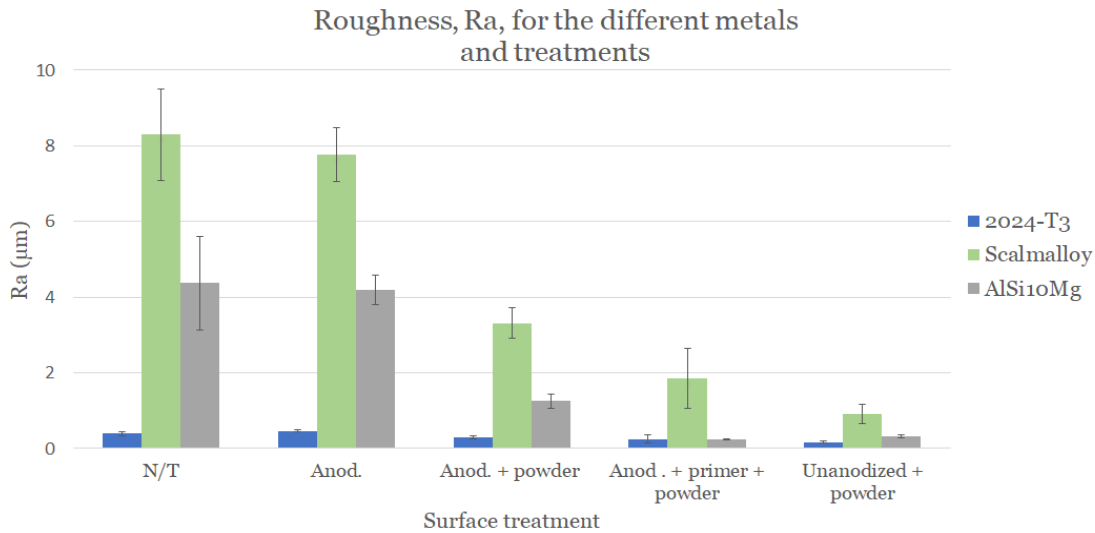
Figure 5.11: *A comparison of Ra [μm] between the samples and surface treatments. The different staples show the Rz-values after a surface treatment. N/T stands for No treatment, which means that the samples have not been surface treated.*
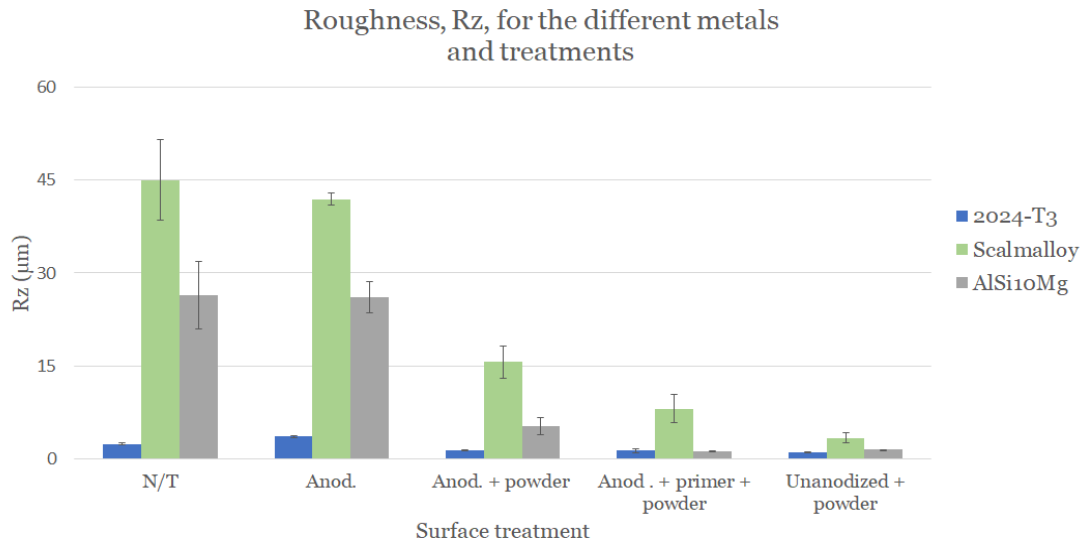
Figure 5.12: *A comparison of Rz [μm] between the samples and surface treatments. The different staples show the Rz-values after a surface treatment. N/T stands for No treatment, which means that the samples have not been surface treated.*

5.5 Blasted samples

The workflow for the blasted samples was the same as for the raw samples and is illustrated in Figure 4.1. The anodization was done according to procedure, where the alloys were anodized together, in the same conditions as described above in the experimental section for all alloys. The images shown in Figure 5.13, were conducted by Dino-Lite Digital Microscope, and were taken before and after anodization. The upper images, B3 and C3, in Figure 5.13 shows the blasted surface of Scalmalloy® and AlSi10Mg before any pretreatments or anodization were performed, and the lower images, B4 and C4, shows the blasted surface sample after pretreatments and anodization.
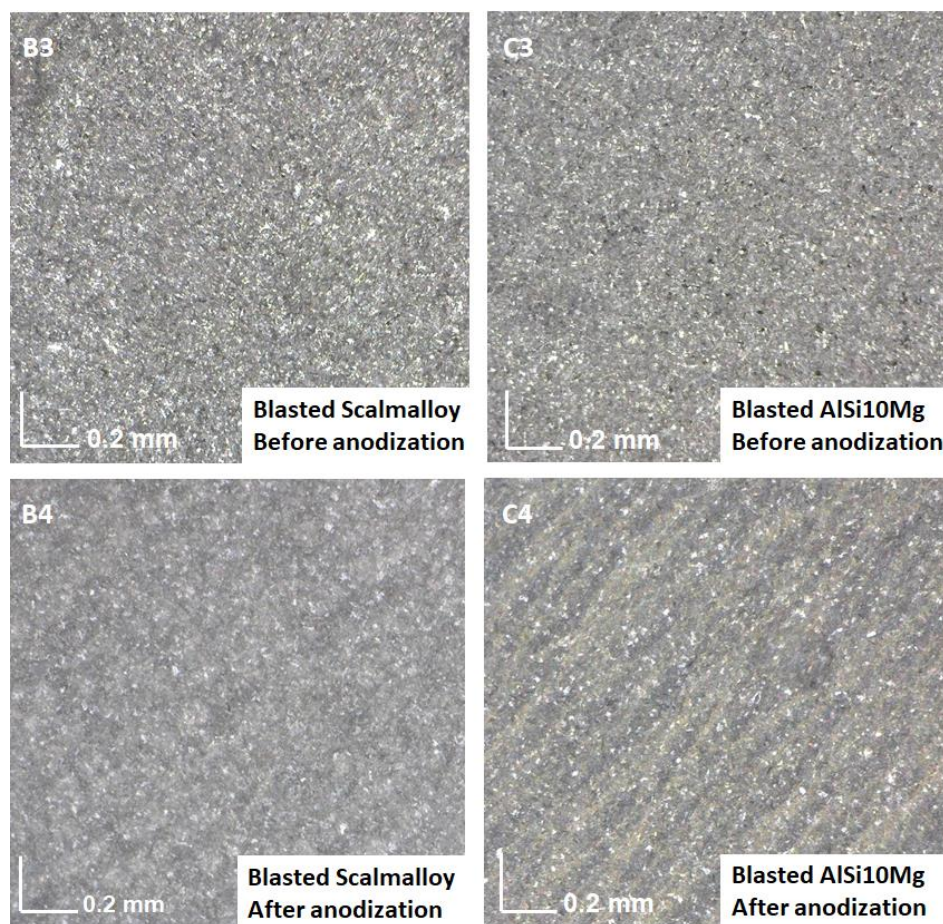
Figure 5.13: *Dino-Lite Digital Microscope image with the magnification 180×. B3) Scalmalloy® before undergoing any pretreatments or anodizing. C3) AlSi10Mg before undergoing any pretreatments or anodizing. B4) Scalmalloy® after anodization. C4) AlSi10Mg after anodization.*

The images given from contact angle goniometry were compared and evaluated. In Figure 5.14, a selection has been made according to the images which in a most representative way shows the wettability of the anodized blasted samples. Next to the pictures, the calculated CA-values from each measurement are shown.

Sample	CA [o]
Scalmalloy®	0
AlSi10Mg	< 10
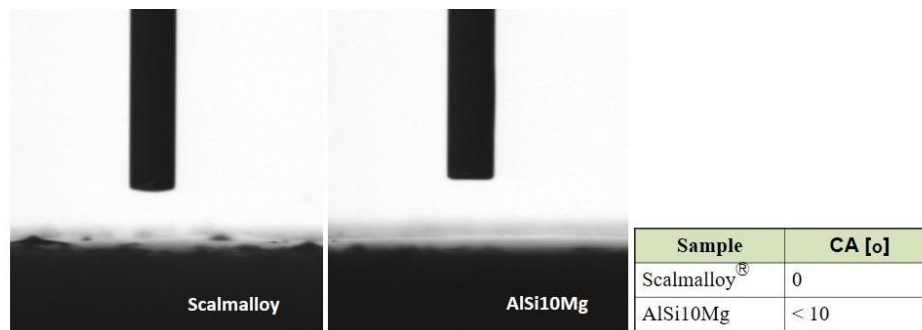
Figure 5.14: *Shows the nature of the droplet on blasted and anodized Al alloys according to procedure 1, where samples were anodized together. In both cases, a droplet cannot be identified on the surface and no CA was calculated.*

The SEM measurement for the blasted and anodized alloys are shown in Figure 5.15. Pore diameter, interpore distance, pore wall thickness and porosity were measured and calculated by using ImageJ. The results measured and calculated by ImageJ are presented in Table 5.2.
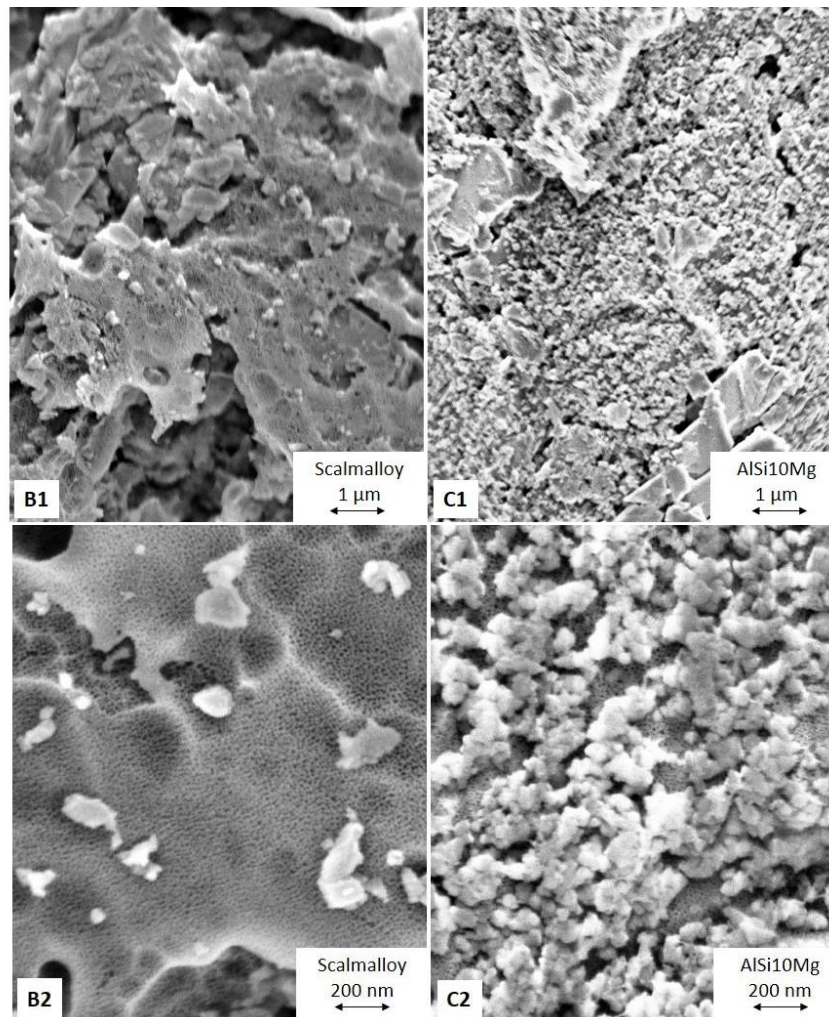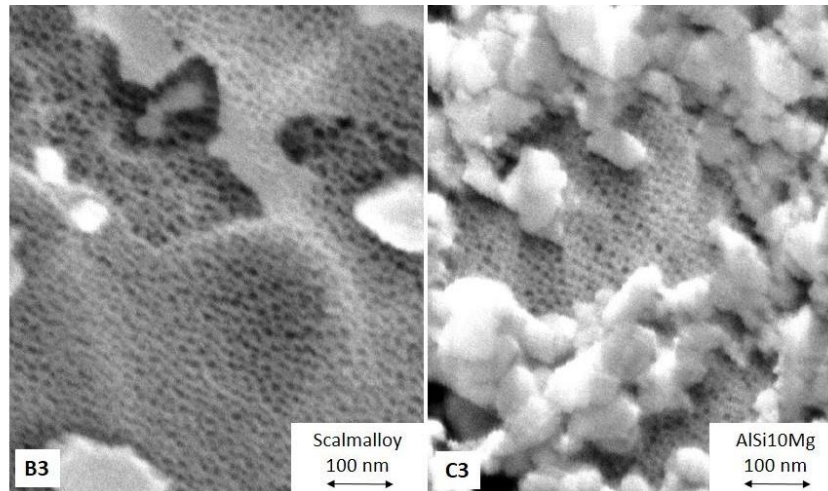
Figure 5.15: *Images received from SEM of blasted samples, where B=Scalmalloy®, C=AlSi10Mg, 1=magnification 25 000x, 2=magnification 120 000x and 3=magnification 300 000x.*

Table 5.2. *Values of the morphology parameters: pore diameter, interpore distance, pore wall thickness and porosity of the blasted alloys.*

Blasted sample	Pore diameter [nm]	Interpore distance [nm]	Pore wall thickness [nm]	Porosity [%]
Scalmalloy®	9.7 ± 2.4	20.5 ± 4.9	8.5 ± 3.4	20.4 ± 1.9
AlSi10Mg	9.1 ± 1.2	17.1 ± 2.7	13.7 ± 5.6	17.6 ± 0.8

Also, profilometry was performed for the blasted samples. The *Ra* and *Rz*-values were measured and the results from the measurements are shown in Figure 5.16 and 5.17, in comparison to the raw samples.

43

Roughness, Ra, for blasted AM metals and treatments
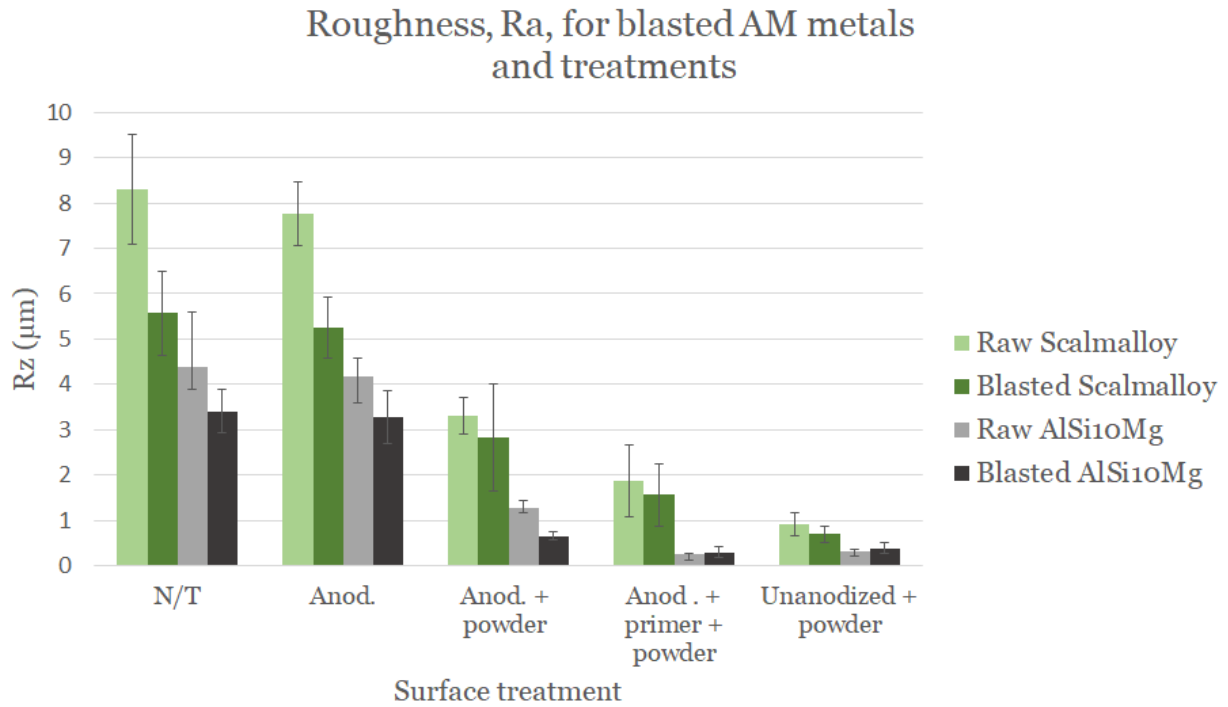
Figure 5.16: A comparison between raw and blasted samples according to the Rz-values. The different staples show the Ra-values after a surface treatment. N/T stands for No treatment, which means that the samples have not been surface treated.

Roughness, Rz, for blasted AM metals and treatments
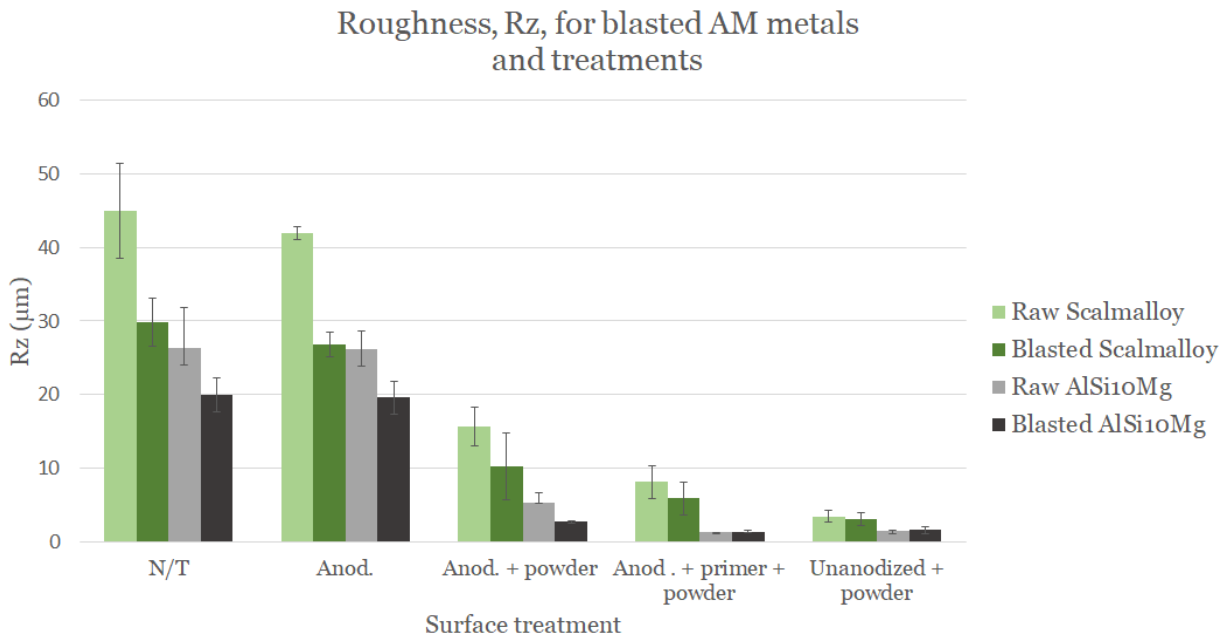
Figure 5.17: A comparison between raw and blasted samples according to the Ra-values. The different staples show the Rz-values after a surface treatment.N/T stands for No treatment, which means that the samples have not been surface treated.

44

6 | Discussion

In this section, a further discussion of the results obtained will be made according to the literature and own experiences.

6.1 Anodization process

After the anodization process, the first observation was a color change. Scalmalloy® became dark and AlSi10Mg became even darker. The color change was further studied using a light microscope, shown in Figure 5.4. Al alloy 2024-T3 did not show a change in color, which is expected due to the previous master thesis conducted by Poot (2019).

In the case of Scalmalloy®, it is suggested that the color change depends on the impurities since a brown and yellow color could be observed before the pretreatments and anodization, and not after. For AlSi10Mg a yellow and goldish surface could be distinguished after anodizing. The composition of the silicon alloy may affect the anodization process and based on these first results, it can be speculated that the anodization process has been affected. According to Zhu (2019), the discoloration can be explained by undissolved Si in the oxide layer, causing anodized Si-alloys look grey and dark for the observers' eye for alloys with Si-content that exceeds 5 wt-%. This may also be the case for Scalmalloy®, but instead there could be due to other intermetallic particles such as Mg. After consultation with working employees, another suggestion is that Si particles in AlSi10Mg have migrated towards the surface, making the surface look more yellow and goldish for the surfaces detected with the light microscope in Figure 5.4. Another suggestion for the yellow color change of AlSi10Mg is that the pickling bath has contributed to a color change, but this is more unlikely since Scalmalloy® did not prove for a yellow color after the anodization process.

In this master's thesis, the anodization of the AM alloys was conducted in two different procedures, one where the three alloys were anodized together and another one where the samples were anodized separately - procedure 1 and 2 respectively. When anodizing the alloys according to procedure 2, the respective properties of the alloys can be investigated and understood in a better way. Due to the speculation of the particle's movement or inhibition, it was of interest to separately investigate the current when anodizing the alloys. If particles have migrated towards the surface or if the oxide film contains undissolved particles, it is possible that they inhibit the production of oxide film during the anodization and thereby resulting in a thinner layer of anodic coating. From Figure 5.3, it can be observed that the Al alloy 2024-T3 and AlSi10Mg have a smaller current compared to the Scalmalloy®. The variation in current, and thereby the current density, may depend on the differences in surface structure and area. The AM alloys, Scalmalloy® and AlSi10Mg exhibits a rougher surface structure than Al alloy 2024-T3 (Fig 5.11), a trend that is most evident for Scalmalloy®. A rougher surface structure resulting in a

larger surface area, possibly creates the higher value of the current for Scalmalloy. For all three samples, the current shows a similar decreasing trend, indicating that an anodic coating is built up and the resulting insulating anodic layer reduces the current. The graphs for Al alloy 2024-T3 and AlSi10Mg reaches a steady state after 5-10 minutes while Scalmalloy® keep descending, indicating that the anodic build-up was ceased for Al alloy 2024-T3 (Jani *et al.,* 2013) and AlSi10Mg but still under progress after the time limit for Scalmalloy®. Further, this could also indicate that the Al alloy 2024-T3 and AlSi10Mg have created a thinner anodic coating compared to Scalmalloy® due to the continuing declining current for Scalmalloy®.

The results from the profilometry measurements indicated that *Ra* and *Rz* are increased after anodization for the Al alloy 2024-T3. According to the studies by Thompson (1999) and Vargel (2004), the morphology is modified during the anodization and a porous oxide layer is created. The obtained rougher surface for Al alloy 2024-T3 indicates that a porous oxide layer has been created and the anodization has been done successfully. For the AM alloys, a small decrease in *Ra* and *Rz* can be observed. This decrease in roughness is explained by the anodization making the AM surfaces smoother. However, it is difficult to speculate since the difference is very small.

During the anodization process, some error sources in the performance and instruments can be identified. According to the Saab AB's standard, the temperature and voltage is supposed to be set at 39 °C and 14 V. Due to the homemade anodization setup, there were some difficulties of controlling the temperature and voltage precisely. During the anodization process, some energy is released in the form of heat, making it difficult to control the temperature of the TSA when using a regular heating plate. The multimeter used for controlling the voltage was manually set, creating difficulty in setting the desired voltage to high precision. However, the variation was very small and probably has not affected the results.

6.2 Wettability

Investigating the wettability for the surface of AM alloys is interesting to understand the adhesion properties of a surface (Guo et al, 2013). The L-PBF process produces rough surfaces, resulting in rougher surfaces of the AM AlSi10Mg and Scalmalloy® compared to the reference material Al alloy 2024-T3 (Cheng and Chou, 2015). Therefore, the wettability of the surface of different samples has been estimated with contact angle goniometry and were measured before and after the anodization process for all the alloys. In Figure 5.5, a visible droplet for all the surfaces is observed and it can be shown in the attached table that the CA for both the Al alloy 2024-T3 and AlSi10Mg is high with a high standard deviation. For Scalmalloy®, one droplet is identified, but the software could not find the baseline, making it hard to calculate CA for this surface. When comparing the droplet with the other measurements one can assume that the droplet has a similar value as AlSi10Mg due to the similarities of the formed droplet.

After the anodizing process, a droplet for the Al alloy 2024-T3 can be identified meanwhile there is no droplet to be found for the AM samples. This indicates that the wettability for the AM samples are higher compared to Al alloy 2024-T3. In the attached tables in Figure 5.6 and 5.7, the CAs for the AlSi10Mg and Scalmalloy® are equal or close to 0°, indicating that the surfaces are completely wettable ($\theta = 0$) for both anodized and raw AM surfaces. When observing the CA measurements and images more closely, one could observe that the droplet spread out over the whole surface of Scalmalloy® and evaporated shortly after the droplet was placed on the surface. In comparison to Scalmalloy®, the droplet on AlSi10Mg was spread out at a slower rate and not in the same extension. As mentioned earlier, the anodization process was conducted in two different procedures and some differences in CAM on the AM samples could be obtained when the alloys were anodized together compared to when the samples were anodized separately. In Appendix III, one can see that small droplets can be identified for the AM Al alloys which were anodized separately. Additionally, there were also cases where no droplets were formed on the same surface. However, if a droplet could be found the CA was very small for the droplet and the surfaces can be concluded as wettable.

There is a large difference in the roughness between the AM samples compared to Al alloy 2024-T3, which can be seen in the bar graphs in Figure 5.11 and 5.12. The surface of Al alloy 2024-T3 is smoother and could be described as an even surface, making Al alloy 2024-T3 to be considered to be in the Young state for perfectly flat and rigid surfaces. The AM samples are more of an uneven surface and could considered to be in the Wenzel state due to the high roughness. It seems that the placed droplets on the AM samples penetrate the irregularities in the surfaces. When studying the formation and the spread of the droplet on the anodized AM samples, it seems that the wettability is even higher for Scalmalloy® compared to AlSi10Mg. It could be concluded that the AM samples have a higher wettability compared to Al alloy 2024-T3, meaning that an increasing roughness decreases the CA. A suggestion could be that the roughness together with the formed porous oxide layer leads to more irregularities for the droplet to penetrate on the AM samples surfaces, making the surface more wettable.

The adhesion properties could be correlated to the surface wettability, and according to Guo et al. (2013), the wettability is dependent on the porous structure of the formed oxide layer during anodizing. It is advantageous to have good adhesion properties when painting a metal surface. In our case, the low CAs for the AM samples indicate that the surfaces probably will have good adhesion properties, before and after anodization. As for Al alloy 2024-T3, good adhesion properties are shown after anodization.

The investigation of the relationship between wettability and morphology was studied by Poot (2019) and a suggestion is that the low CA could be explained by high porosity. In the study, Poot mentions that higher porosity could be an indication of thin pore walls failing to support the liquid droplet. In Table 5.1, the porosity is highest for the 2024-T3 alloy, which also has smaller

pore wall thickness compared to the AM samples. Hypothetically, this would make Al alloy 2024-T3 more wettable compared to the AM samples. In summary, it could be concluded that other parameters, such as the difference in roughness, may play crucial roles in the wettability and thereby the adhesion properties.

During CAM, some error sources in the performance and instruments can be identified. Several droplets could not be measured due to the difficulty for the software to find the baseline and thereby calculating CA, even if the observer's eye could identify the droplets. One explanation could be that the high roughness of the AM samples makes it challenging for the CAM instrument to distinguish the droplet from the surface.

6.3 Morphology of the anodic coating for the different metals

Before the SEM measurement, the samples were sputtered with Pt. When comparing the sputtered samples with the untreated samples, a darker color could be observed. The dark coating indicated that the sputtering step was done properly. Later, during the SEM measurements, it was difficult to enlarge the images due to moving samples, making it hard to create sharpness in the images to further make enlargements. However, desired enlargements were made and the magnification for the samples were measured to be 25 000 ×, 120 000 × and 300 000 ×.

SEM measurements were done to obtain knowledge about the morphology of the anodized surfaces and the anodic coatings for the AM samples. When looking at Figure 5.8 and the images A1, B1 and C1, a clear difference in microstructure is shown. This was expected due to the studies discussing that there is a difference in the microstructure between AM metals and conventional metals (Revilla *et al.*, 2019). Al alloy 2024-T3 shows a smooth surface while Scalmalloy$^®$ and AlSi10Mg exhibits a rough surface, and once again the differences in Ra and Rz from the profilometry are proven. In the pictures, a pore structure can be observed for Al alloy 2024-T3 but in the case for Scalmalloy$^®$ and AlSi10Mg, no pore structure can be observed at this scale.

When looking at larger magnifications, 120 000 × and 300 000 ×, it is possible to distinguish a pore structure for all alloys. An interesting observation is that AlSi10Mg have two surface layers, and that the lower layer is anodized while the upper layer does not show the characteristic structure of an anodic coating. This may originate from the manufacturing technique, the alloys composition, or a combination of both. Since Scalmalloy$^®$ shows a porous structure and has similar manufacturing techniques as AlSi10Mg, it is more likely an effect of the composition and the Si-particles. A study conducted by Zhu et al. (2019) suggests that the Si has an impact on the anodization due to that Si-particles are not dissolved or anodized at the same rate as Al. Other studies have confirmed that Si-particles have an impact on the anodic coating on AM AlSi10Mg as well and this could result in a different porous structure, pore diameter and growth of the oxide

layer (Revilla *et al.* 2017; Revilla *et al.,* 2019). Based on this knowledge, this may be the reason why there are two different layers for AlSi10Mg. However, further investigation is needed to understand what the upper layer on AlSi10Mg consists of.

In summary, when comparing the anodic coating of Scalmalloy® and AlSi10Mg, it is observed that larger parts for Scalmalloy® have been anodized, even in the darker areas which can be seen in Figure 5.8 in picture B2. Overall, the pictures from SEM indicate a successful anodization with TSA and from a health perspective, this is very desirable because it enables Saab AB to continue their chromate-free surface treatment if implementing AM alloys in their manufacturing in the future.

Morphology parameters
From the SEM images it was possible to calculate the pore diameter, pore wall thickness and porosity by using ImageJ. The pore diameter is highest for Al alloy 2024-T3 and the lowest for AlSi10Mg. The pore wall thickness is smallest for Al alloy 2024-T3 and highest for AlSi10Mg. When comparing the pore diameter and pore wall thickness with the calculated porosity, two conclusions can be made. Firstly, a larger pore wall thickness and a larger pore diameter proves for a lower porosity, as for AlSi10Mg. Secondly, a smaller pore wall thickness and a smaller pore diameter proves for a higher porosity, as for Al alloy 2024-T3. This is a good result as it is in line with theory. The porosity is an indication of the number of pores, and if the pore diameter as well as the pore wall thickness is small, there is room for a higher number of pores on the surface. By looking closely at the pictures in Figure 5.8 the correlation between the calculated morphology parameters matches the correlation between the observed morphology in the pictures, which also proves for good and reliable results from ImageJ.

In several studies the correlation between different anodizing parameters and the anodic coating morphology has been investigated. It is suggested that an increasing anodization temperature contributes to an increased pore size and thus an increased porosity. It is also discussed that film porosity contributes to the corrosion resistance of the anodic film, and that a reduced porosity also may indicate that there is a reduced dissolution of the anodic film. (Ma *et al.,* 2016) According to the study conducted by Ma et al. (2016) it seems that the reduced porosity could contribute to an improved corrosion resistance. This could indicate that the gained lower porosity for Scalmalloy® and AlSi10Mg could be of advantage when it comes to corrosion resistance. However, as mentioned earlier there are areas of the AM samples that are not anodized, making the anodization not uniformed. This may contribute to a non-protective anodic coating and cause the surface more prone to corrosion.

Overall, the pore structure for Scalmalloy® and AlSi10Mg is very similar to Al alloy 2024-T3, proving for a honeycomb structure being created for the AM samples. Also, these similarities may prove for similar adhesion and corrosion properties as for the Al alloy 2024-T3. However,

the process parameters need to be varied in order to precisely discuss the effect of the porosity and the pore structure.

There were several difficulties by using ImageJ. In order to clearly calculate the different parameters, it is of high importance that the pictures have good sharpness. By using slightly unsharp images, it is easy to confuse what is a pore and what can be roughness or a shadow, resulting in misleading results. Moreover, the software could not calculate the pore diameter, interpore distance, pore wall thickness and porosity at the same time, causing it impossible to measure all parameters for one specific pore. This is very desirable since this would give the best representative result possible for the porosity.

6.4 Powder coating

In this study, there was also an investigation of the AM samples adhesion properties for powder coating. The powder coating experiment was performed on several different surfaces with different treatments, which is shown in Table 4.3. Thereafter, the thickness of the powder coating for our reference material was measured to 41 μm. According to the Saab AB standard, the powder coating should be in the interval of 30 - 60 μm. Since the instrument that measures the thickness of the applied powder coating was not able to measure the thickness for the AM samples, the thickness was assumed to be the same as for the reference alloy.

Different adhesion tests were conducted on all the powder coated surfaces, to investigate if the powder coating would be affected. The only test that showed diverse results was the adhesive test performed after the samples had been immersed in a water bath for 24 hours. For the raw 2024-T3 alloy, the powder coating was released from the surface, but for all the other surfaces the powder coating was still attached, proving for good adhesion for this powder coating.

The anodization is performed to improve the corrosion and to improve the adhesion properties for the metal (Vargel, 2004). When it comes to the AM samples, it seems that the powder coating is attached to the surface regardless whether the metal surface is anodized or not, with or without primer. When comparing the difference roughness for the different metals, one can see in the bar graphs in Figure 5.11 and 5.12, that the roughness is very high before and after anodization for the Scalmalloy® and AlSi10Mg when comparing it to our reference material 2024-T3. Thus, it could be concluded that the metal's properties, such as the roughness, plays a crucial part in this good adhesion properties, besides from the high wettability, for the AM samples. When studying the bar graphs in Figure 5.11 and 5.12, the surface roughness for both the AM samples has decreased drastically for both the *Ra* and *Rz*-values. This indicates that the powder coating makes the AM surfaces smoother, which is a desirable property for the finished product. However, the lowest *Ra* and *Rz* are found for unanodized AM samples with powder coating, which is explained by a higher conductivity for the surfaces which do not have the insulating oxide layer.

Overall, it seems that most of the surfaces have good adhesion properties for powder coating, making powder coating a very good substitute to wet paint. From the results, a speculation in a replacement of wet paint coating with powder coating can be made for Saab AB. If wet paint could be replaced by powder coating this will have an environmental advantage due to the powder coating being VOC-free. Furthermore, in order to implement this substitute, further corrosion tests are needed to be done.

6.5 Blasted samples

It is suggested by Revilla et al. (2019), that the surface roughness and post-treatments such as blasting, has effects on the morphology of the porous oxide layer. Therefore, an investigation was done to compare raw AM alloys with blasted AM alloys. The experimental parts for the blasted alloys were done in the same way as for the raw alloys and majority of the results showed similar trends. From the anodization, the same color change could be observed but due to a finer surface structure, it is more difficult to distinguish. From the profilometry, the same trend could be observed except for smaller values, which is as expected since the purpose of a blasting process is to smoothen a surface. From CAM, no significant difference could be observed since no droplet could be identified for these samples as well. However, a dissimilarity can be observed when comparing the SEM images and morphology parameters.

The AM samples showed a porous structure after anodization. When comparing blasted Scalmalloy® with raw Scalmalloy®, the surface and pore structure are very similar, but for AlSi10Mg the surfaces have a different structure. The surface for raw AlSi10Mg is segmented in two surface layers. The lower layer exhibiting the characteristic anodic structure is possible to be distinguished in its raw form but for the blasted AlSi10Mg, this lower layer can't be distinguished due to the upper layer being more dense covering the lower layer. The blasting process results in smaller visible areas for the lower layer, which can be problematic since it was discovered that only the lower layer was anodized. Smaller visible areas for the lower layer may thereby contribute to unsuccessful anodization. As discussed earlier, it seems that the anodization step is unnecessary for the adhesion properties when powder coating, making this unsuccessful anodization unnecessary as well. Moreover, the pore structure in the lower layer is similar for the blasted and raw AlSi10Mg.

The morphology parameters from ImageJ differs between raw and blasted AlSi10Mg but not for Scalmalloy®. For AlSi10Mg, the porosity is higher for the blasted sample compared to the raw sample. Probably, this difference originates from the artificial factor when using ImageJ. Blasted AlSi10Mg has less anodized areas, making it difficult to measure a representative pore diameter, interpore distance, pore wall thickness and porosity. From the powder coating, the blasted samples exhibit the same behaviors as for the raw samples.

7 | Future Work

The work in this master thesis was focused on gaining more knowledge about the morphology of the anodic coating and adhesion properties for powder coating for the AM alloys Scalmalloy$^{®}$ and AlSi10Mg. However, the work has also raised new questions and left questions unanswered. The use of AM Al for aircraft applications is in a development phase and further investigation of the anodic coating and corrosion resistance is needed to be done in order to be used on a larger scale.

7.1 The anodization procedure

A comparison between the anodization process in lab-scale and Saab AB's production was also conducted in this master thesis. The results showed that the morphology of the anodic coating for Al alloy 2024-T3 was different when comparing the anodization in lab-scale with production. Future work could include performing similar tests at production scale for the AM samples and then compare it to the laboratory scale, in order to observe any differences in the morphology for the AM samples

For the conventional alloy 2024-T3, the porous structure is related to anodization process parameters such as voltage, time, temperature, and electrolyte type. The anodization for this alloy is well understood. For AM alloys, the anodizing mechanism has not been studied to the same extent. Thus, changing and varying process parameters should be done to get a better understanding of the anodization behaviors of AM alloys. According to studies, the applied voltage and current density has a great impact on the formed anodic coating. During the anodization process, a difference in current was observed for the different alloys when applying the same voltage. The AM samples have a rougher surface resulting in a larger surface area, making it interesting to vary the applied voltage in the system and investigate the effect of the current density. It would also be of interest to investigate the choice of electrolytic solution, since Al-Mg alloys are often anodized in alkaline solutions instead of acidic solutions.

7.2 Further study on the morphology of the anodic coating

Due to varied measured current between the alloys when performing anodization according to procedure 2, further studies of the morphology of the anodic coating is of interest. As future work, it is suggested to investigate the thickness of the produced oxide film by observing a cross section of the samples in TEM. It is discussed that AlSi10Mg and Al alloy 2024-T3 have created a thinner oxide film compared to Scalmalloy$^{®}$. By observing samples cross section these speculations can be confirmed.

7.3 Characterization with EDX

In order to clarify the alloy's elemental composition and quantitative compositional information, it is recommended to execute EDX, Energy-dispersive X-ray spectroscopy. EDX is an analytical technique used for identifying elements and chemicals of a sample and can be done in a properly equipped SEM. The EDX analysis can be used to determine the elemental composition and the lateral distribution from the imaged area (Sebnesajjad, 2014). By using EDX it is possible to distinguish Si and Mg particles in the alloy and the oxide film, and this can give an understanding of the possible inhibition of Si and Mg during anodization.

7.4 Further investigation of powder coating properties

The adhesion tests performed in this thesis gives a first indication of the samples' corrosion properties. However, tougher adhesion and corrosion tests need to be executed. As future work it is suggested to execute a filiform corrosion test and a pull-off test. The principle of filiform corrosion test is to scribe the surface of the sample, place the sample in a corrosive environment to initiate corrosion and expose the sample to a controlled temperature and humidity conditions conducive to filiform corrosion. The filiform corrosion test may vary in length. The longer the test is run, the harder the test is and vice versa. To begin with, it is of interest to start with a 1000-hour long filiform test in order to further increase the time limit until all samples are destroyed. The pull-off test is done by properly attaching a stub to the surface and then pulling it off while the required force is measured giving information about the adhesion force between the paint and the substrate. Due to the size of the stub, larger samples are required.

8 | Conclusion

The first results from the experimental parts showed a color change after anodization for AlSi10Mg and Scalmalloy®, which probably originates from undissolved particles in the surface. Scalmalloy® has the roughest morphology compared to the other Al alloys, both before and after anodization. The observed current indicated a maximum anodic build-up for Al alloy 2024-T3 and AlSi10Mg but still under progress after 20 minutes for Scalmalloy®. The profilometry measurements demonstrate an increasing roughness after the anodization for Al alloy 2024-T3, and a very small decreasing roughness for the AM samples.

The study shows that a porous structure has been formed. However, comparing the AM samples with the reference material 2024-T3, some dissimilarities in the anodic coating structure could be identified. It could be concluded that an uniformed oxide layer has not been formed for AlSi10Mg. It is suggested that the different anodic coating is formed due to intermetallic particles disrupting the anodization. Overall, the study shows that a porous structure similar to the reference material 2024-T3, is formed for the AM samples, especially for Scalmalloy®. This could further indicate that the AM samples could have similar properties as the reference material that is used at Saab AB.

From the CA measurements, it can be concluded that the AM alloys have a higher wettability compared to the conventionally produced Al alloy 2024-T3, although the margins are small. Also, it is suggested that the roughness is correlated to the wettability since a high roughness proved for a higher wettability. The high wettability for both raw and anodized AM surfaces indicates good adhesion properties.

The results from powder coating showed that the AM surfaces have a smoother finish after the powder coating step. It is concluded that the roughness of the metal plays a crucial part in the adhesion properties due to the powder coating being attached for surfaces that did not undergo anodization. Thus, it could be suggested that anodization is not necessary in order to improve the adhesion properties for AM metals. Further investigation of the corrosion resistance is required to determine if the anodization step is needed for AM alloys that will be powder coated.

Most of the results from the blasted samples proved for similar trends as for the raw samples, except for the SEM images where AlSi10Mg showed a different surface structure.

9 | References

Abrahami, S. T. *et al.* (2017) 'Towards Cr(VI)-free anodization of aluminum alloys for aerospace adhesive bonding applications: A review', *Frontiers of Chemical Science and Engineering*, pp. 465–482. doi: 10.1007/s11705-017-1641-3.

Accretech Tokyo Seimitsu (no date) 'Surface Texture - Contour Measuring Instruments', pp 230-237. Available at: https://static1.squarespace.com/static/5155d3e7e4b01a74bb7d1208/t/56c0c7e960b5e9bcb0044108/1455474673174/SurfaceFinishExplain+-+Accretech.pdf (Accessed: 24 March 2020)

apworks (2019) *Scalmalloy®*, *Home*. Available at: https://apworks.de/en/scalmalloy/ (Accessed: 29 January 2020)

apworks (2019) *Scalmalloy®*, Material Sheet. Available at: https://www.apworks.de/wp-content/uploads/2015/07/20160401_SCALMALLOY_REV0005.pdf?fbclid=IwAR33spLar6zoLbpgUE9Ao0k0C0301f_guuXMkJigNSMJTB9Q4bXHvuKy55k (Accessed: 7 May 2020)

Attaran, M. (2017) 'The rise of 3-D printing: The advantages of additive manufacturing over traditional manufacturing', *Business Horizons*, pp. 677–688. doi: 10.1016/j.bushor.2017.05.011.

Awd, M. *et al.* (2017) 'Comparison of Microstructure and Mechanical Properties of Scalmalloy® Produced by Selective Laser Melting and Laser Metal Deposition', *Materials*. MDPI, 11(1). doi: 10.3390/ma11010017.

Barboriak, D. P. et al. (2005) 'Creation of DICOM—Aware Applications Using ImageJ', Journal of digital imaging. Springer, 18(2), p. 91.

Barnes, G., & Gentle, (2005). 'Interfacial Science: An introduction' (2 ed). New York: Oxford University Press Inc.

Bartlett, J. L. and Li, X. (2019) 'An overview of residual stresses in metal powder bed fusion', *Additive Manufacturing*, pp. 131–149. doi: 10.1016/j.addma.2019.02.020.

Cabrini, M. *et al.* (2016) 'Evaluation of corrosion resistance of Al–10Si–Mg alloy obtained by means of Direct Metal Laser Sintering', *Journal of Materials Processing Technology*, pp. 326–335. doi: 10.1016/j.jmatprotec.2015.12.033.

Cheng, B. and Chou, K. (2015) 'Melt Pool Evolution Study in Selective Laser Melting', in *26th Annual International Solid Freeform Fabrication Symposium - An Additive Manufacturing Conference*. unknown. Available at: https://www.researchgate.net/publication/283017877_Melt_Pool_Evolution_Study_in_Selective_Laser_Melting (Accessed: 24 March 2020).

Critchlow, G. W. *et al.* (2006) 'Strategies for the replacement of chromic acid anodising for the structural bonding of aluminium alloys', *International Journal of Adhesion and Adhesives*, pp. 419–453. doi: 10.1016/j.ijadhadh.2005.07.001.

Clean Sky (no date) *Saab Corporate*. Available at: https://saabgroup.com/responsibility/reduce-the-environmental-impact/sustainable-innovations/clean-sky/ (Accessed: 20 March 2020).

DinoCapture User Guides (no date). Available at: https://www.dinolite.us/dl/dnc2help_en.pdf (Accessed: 24 March 2020).

Edström, A. and Målberg, S (2018) 'The strategic research agenda for the Metal Manufacturing Industry'. Available at: https://www.diva-portal.org/smash/get/diva2:1263216/FULLTEXT01.pdf (Accessed: 11 May 2020).

EOS M 290 'Aluminium AlSi10Mg' (no date). Available at: https://cdn0.scrvt.com/eos/public/8837de942d78d3b3/4e099c3a857fdddca4be9d59fbb1cd74/EOS_Aluminium_AlSi10Mg_en.pdf (Accessed: 25 March 2020).

Epa, U. S. and OAR (2014) 'Volatile Organic Compounds' Impact on Indoor Air Quality'. Available at: https://www.epa.gov/indoor-air-quality-iaq/volatile-organic-compounds-impact-indoor-air-quality (Accessed: 23 April 2020).

Gardan, J. (2016) 'Additive manufacturing technologies: state of the art and trends', *International Journal of Production Research*, pp. 3118–3132. doi: 10.1080/00207543.2015.1115909.

Gharbi, O. *et al.* (2018) 'Chromate replacement: what does the future hold?', *npj Materials Degradation*. Nature Publishing Group, 2(1), pp. 1–8.

Gu, X.-H. *et al.* (2020) 'Corrosion Behavior of Selective Laser Melted AlSi10Mg Alloy in NaCl Solution and Its Dependence on Heat Treatment', *Acta Metallurgica Sinica (English Letters)*, pp. 327–337. doi: 10.1007/s40195-019-00903-5.

Guo, C., Wang, X.-W. and Yuan, Z.-H. (2013) 'Pore diameter-dependence wettability of porous anodized aluminum oxide membranes', *Journal of Porous Materials*, pp. 673–677. doi: 10.1007/s10934-012-9641-7.

Gupta. R.C. (2019) *Biomarkers in Toxicology | ScienceDirect*. Available at: https://www.sciencedirect.com/book/9780128146552/biomarkers-in-toxicology (Accessed: 25 March 2020).

ImageJ (no date) *ImageJ*. Available at: https://imagej.net/ImageJ (Accessed: 24 March 2020).

Introduction ImageJ (no date). Available at: https://imagej.nih.gov/nih-image/about.html (Accessed: 24 March 2020).

Ilango, M. S., Mutalikdesai, A. and Ramasesha, S. K. (2016) 'Anodization of Aluminium using a fast two-step process', *Journal of Chemical Sciences*, pp. 153–158. doi: 10.1007/s12039-015-1006-8.

Jani et al (2013) 'Nanoporous anodic aluminium oxide: Advances in surface engineering and emerging applications', Progress in Materials Science. Pergamon, 58(5), pp. 636–704.

Juhl, A.D. (1998) 'Comparison of the Anodic Oxide Layer Formed on five Sand Cast Aluminum Alloys', in: IHAA 7th International Conference, San Diego, USA.

Kahlin, M. *et al.* (2017) 'Fatigue Performance of Additive Manufactured Ti6Al4V in Aerospace Applications'. doi: 10.3384/lic.diva-137233.

Kikuchi, T. *et al.* (2015) 'Porous Aluminum Oxide Formed by Anodizing in Various Electrolyte Species', *Current Nanoscience*, pp. 560–571. doi: 10.2174/1573413711999150608144742.

Kim, B. R. (2011) 'VOC Emissions from Automotive Painting and Their Control: A Review', *Environmental Engineering Research*. 16(1), pp. 1–9.

Laurén, S. (no date) *What is adhesion?* Available at: https://blog.biolinscientific.com/what-is-adhesion (Accessed: 10 April 2020)

Leon, A. and Aghion, E. (2017) 'Effect of surface roughness on corrosion fatigue performance of AlSi10Mg alloy produced by Selective Laser Melting (SLM)', *Materials Characterization*, pp. 188–194. doi: 10.1016/j.matchar.2017.06.029.

Li, S.-M. *et al.* (2015) 'Effect of intermetallic phases on the anodic oxidation and corrosion of 5A06 aluminum alloy', *International Journal of Minerals, Metallurgy, and Materials*. Springer, 22(2), pp. 167–174.

Lin, Y. *et al.* (2018) 'Recent Progress in Preparation and Anti-Icing Applications of Superhydrophobic Coatings', *Coatings World*. Multidisciplinary Digital Publishing Institute, 8(6), pp. 208.

Ma, Y *et al.* (2016) 'Effect of anodizing parameters on film morphology and corrosion resistance of AA22099 aluminum-lithium alloy' *Journal of electrochemical society,* 163(7) pp. C369-C376. doi: 10.1149/2.1081607jes]:

Makkonen, L. (2016) 'Young's equation revisited', *Journal of Physics: Condensed Matter*, p. 135001. doi: 10.1088/0953-8984/28/13/135001.

Maldonado, C. *et al.* (2009) 'Evaluation of the Effects of Powder Coating Cure Temperatures on the Mechanical Properties of Aluminum Alloy Substrates', *Journal of Materials Engineering and Performance*, pp. 70–78. doi: 10.1007/s11665-008-9256-y.

Manisalidis, Ioannis et al. "Environmental and Health Impacts of Air Pollution: A Review." *Frontiers in public health* vol. 8 14. 20 Feb. 2020, doi:10.3389/fpubh.2020.00014

Manufacturing Guide Sweden AB (no date). *Pulverlackering*. Available at: https://www.manufacturingguide.com/sv/pulverlackering (Accessed: 6 April 2020)

Marcham, C.L, Walter, A. (2020) 'Environmental Advantages of ADDITIVE MANUFACTURING', Professional Safety. Vol. 65 Issue 1, p34-38. Available at: https://eds.a.ebscohost.com/eds/pdfviewer/pdfviewer?vid=1&sid=0a36858e-829e-492c-80d4-51c063ae9cf8%40sessionmgr4007 (Accessed: 25 March 2020)

Miller, W. S. *et al.* (2000) 'Recent development in aluminium alloys for the automotive industry', *Materials Science and Engineering: A*, pp. 37–49. doi: 10.1016/s0921-5093(99)00653-x.

Mishra, S. and Bharagava, R. N. (2016) 'Toxic and genotoxic effects of hexavalent chromium in environment and its bioremediation strategies', *Journal of environmental science and health. Part C, Environmental carcinogenesis & ecotoxicology reviews*, 34(1), pp. 1–32.

Mower, M.T. and Long, M.J. (2016) 'Mechanical behavior of additive manufactured, powder-bed laser-fused materials' (2016) *Materials Science and Engineering: A*. Elsevier, 651, pp. 198–213.

Mouritz, A. (2012) 'Introduction to Aerospace Materials'. doi: 10.2514/4.869198.

Museux F, Theilmann R (2009) 'Introducing more eco-efficient chemical treatments for aircraft structure - Towards a chromate-free Airbus', *FAST 45 magazine*, pp 2-9.

Nanakoudis, A. (2019) *SEM: types of electrons, their detection and the information they provide*. Available at: https://blog.phenom-world.com/sem-electrons (Accessed: 25 March 2020).

Nationalencyklopedin (no date) 'krom'. Available at: https://www-ne-se.e.bibl.liu.se/uppslagsverk/encyklopedi/l%C3%A5ng/krom (Accessed: 24 March 2020)

Optical Profilometry - Nanoscience Instruments (no date) *Nanoscience Instruments*. Available at: https://www.nanoscience.com/techniques/optical-profilometry/ (Accessed: 24 March 2020).

Poot, T (2019) 'Tuned sustainable anodic coatings for reduced ice adhesion', Master thesis, Linköping University, Linköping.

Revilla, R. I. *et al.* (2017) 'Galvanostatic Anodizing of Additive Manufactured Al-Si10-Mg Alloy', *Journal of The Electrochemical Society*, pp. C1027–C1034. doi: 10.1149/2.1121714jes.

Revilla, R. I. and De Graeve, I. (2018) 'Influence of Si Content on the Microstructure and Corrosion Behavior of Additive Manufactured Al-Si Alloys', *Journal of The Electrochemical Society*, pp. C926–C932. doi: 10.1149/2.0101814jes.

Revilla, R. I., Rojas, Y. and De Graeve, I. (2019) 'On the Impact of Si Content and Porosity Artifacts on the Anodizing Behavior of Additive Manufactured Al-Si Alloys', *Journal of The Electrochemical Society*, pp. C530–C537. doi: 10.1149/2.1351914jes.

Rubben, T., Revilla, R. I. and De Graeve, I. (2019) 'Effect of Heat Treatments on the Anodizing Behavior of Additive Manufactured AlSi10Mg', *Journal of The Electrochemical Society*, pp. C42–C48. doi: 10.1149/2.0371902jes.

Schmidtke, K. *et al.* (2011) 'Process and Mechanical Properties: Applicability of a Scandium modified Al-alloy for Laser Additive Manufacturing', *Physics Procedia*, pp. 369–374. doi: 10.1016/j.phpro.2011.03.047.

Sharifi, M. et al. (2017) 'Preparation and characterization of a high performance powder coating based on epoxy/clay nanocomposite', pp. 69-76. doi: 10.1016/j.porgcoat.2017.02.013.

Singamneni, S. *et al.* (2019) 'Additive Manufacturing for the Aircraft Industry: A Review', *Journal of Aeronautics & Aerospace Engineering*. doi: 10.35248/2168-9792.19.8.215.

Stokes. D (2008) 'Principle and Practice of Variable Pressure/Environmental Scanning Electron Microscopy (VP-ESM)' *John Wiley & Sons.*

Swedish Chemical Agency (no date). Available at: https://www.kemi.se/lagar-och-regler/reach-forordningen/kort-om-reach (Accessed: 20 March 2020).

Tabar, M. A. *et al.* (2019) 'On the applicability range of Cassie–Baxter and Wenzel equation: a numerical study', *Journal of the Brazilian Society of Mechanical Sciences and Engineering*. Springer, 41(10), pp. 1–12.

The Aluminum Association (2015) 'International Alloy Designations and Chemical Composition Limits for Wrought Aluminum and Wrought Aluminum Alloys'

Thompson, G. E. *et al.* (1999) 'Anodizing of aluminium alloys', *Aircraft Engineering and Aerospace Technology*, pp. 228–238. doi: 10.1108/00022669910270709.

Tomassi, P. and Buczko, Z. (2015) 'Electroplating of Nanostructures', in *Electroplating of Nanostructures*. IntechOpen.

Valdesueiro, D. et al. (2017) 'Tuning roughness and gloss of powder coating paint by encapsulating the coating particles with thin Al2O3 films', *Powder Technology*. Elsevier, 318, pp. 401–410. doi: 10.1016/j.powtec.2017.05.019

Vargel, C. (2004) 'The Corrosion Behaviour of Aluminium Alloys', *Corrosion of Aluminium*, pp. 211–230. doi: 10.1016/b978-008044495-6/50016-1.

Veys-Renaux, D., Chahboun, N. and Rocca, E. (2016) 'Anodizing of multiphase aluminium alloys in sulfuric acid: in-situ electrochemical behaviour and oxide properties', *Electrochimica Acta*, pp. 1056–1065. doi: 10.1016/j.electacta.2016.06.131.

Yu, C.-U. *et al.* (2007) 'Pore-size dependence of AAO films on surface roughness of Al-1050 sheets controlled by

electropolishing coupled with fractional factorial design', *Surface and Coatings Technology*, pp. 7259–7265. doi: 10.1016/j.surfcoat.2007.01.033.

Zhu, B. *et al.* (2016) 'A study of formation and growth of the anodized surface layer on cast Al-Si alloys based on different analytical techniques', *Materials & Design*, pp. 254–262. doi: 10.1016/j.matdes.2016.04.013.

Zhu, B. (2019) '*Casting and Anodising of Al Alloys- Alloy Design, Manufacturing Process and Material Properties*', Department of Mechanical and Manufacturing, Jönköping. Available at: http://hj.diva-portal.org/smash/record.jsf?pid=diva2%3A1314611&dswid=-69 (Accessed: 14 April 2020)

10 | Appendix

Appendix I - Statement of authorship

This master thesis was conducted by two students, Karin Andersson and Marianne Gavelius. All experimental work throughout this project, including the experimental planning, execution and analysis has been carried out in collaboration. The writing of the report has been divided in an equal manner. Table A1 presents which student is responsible for each subchapter. It is important to highlight that both students have been involved in editing and revision for all the subchapters.

Table A1. Statement of authorship.

Subchapter	Karin Andersson	Marianne Gavelius
Abstract and Keywords	X	X
Acknowledgment		X
List of abbreviations	X	X
Chemical Denotations	X	X
Introduction	X	X
Purpose	X	
Delimitation	X	
Collaboration partners	X	
Expected impact of study	X	
Project objectives	X	X
Scientific background		
Aluminum alloys		X
Additive manufacturing		X
Corrosion of Al and Al alloys		X
Anodization process		X
Morphology of the anodic coating		X
Parameters affecting the anodic coating	X	X
REACH	X	

Chromium and hexavalent chromium	**X**	
Powder coating	**X**	**X**
Adhesion properties	**X**	
Characterization methods		
Profilometry	**X**	
Dino-Lite Digital Microscope	**X**	
Contact Angle Measurement	**X**	
Scanning Electron Microscopy		**X**
ImageJ	**X**	
Experimental	**X**	**X**
Results	**X**	**X**
Discussion	**X**	**X**
Future work	**X**	**X**
Conclusion	**X**	**X**

Appendix II - Supplementary material from CAM

In Table A2, the average values and the standard deviations from the CAMs of degreased and pickled samples are shown.

Table A2. *Values from CAM measurements for degreased and pickled samples.*

Reference - degreasing	CA [o] ± Std. Dev.
2024 - T3	6.6 ± 2.8
AlSi10Mg	16.3 ± 1.7
Scalmalloy	0 (No droplet identified)
Reference - pickling	**CA [o] ± Std. Dev.**
2024 - T3	12.2 ± 6.5
AlSi10Mg	14.2 ± 3.5
Scalmalloy	0 (No droplet identified)

Appendix III - Wettability for the anodized pieces performed according procedure 2

Contact angle goniometry was also performed for metal surfaces that were anodized according to procedure 2. In this case, a droplet could be identified on certain parts on the AM surfaces. However, the droplet evaporated quickly after a few seconds.
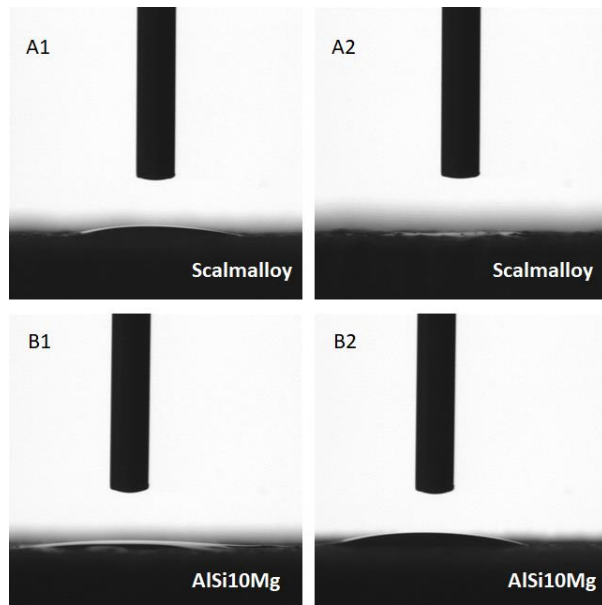
Alloy parts anodized according procedure 2	CA [°]
AlSi10Mg	N/D, no baseline found
Scalmalloy	N/D, no baseline found

Figure A1: *Shows the nature of a droplet on surfaces that has been performed according to procedure 2. For both Scalmalloy® and AlSi10Mg a droplet was identified on certain parts on the surfaces, but the software was not able to perform a CA-calculation.*

Appendix IV – Differing results from SEM

From the SEM measurements of the anodized sufaces, there were some areas on the AM samples that showed different surface morphologies which can be seen in Figure A2. The images B1 and B2 shows Scalmalloy® at different magnifications and C1 show AlSi10Mg. However, these results need to be investigated further in order to clearly understand the deviations on the surfaces.
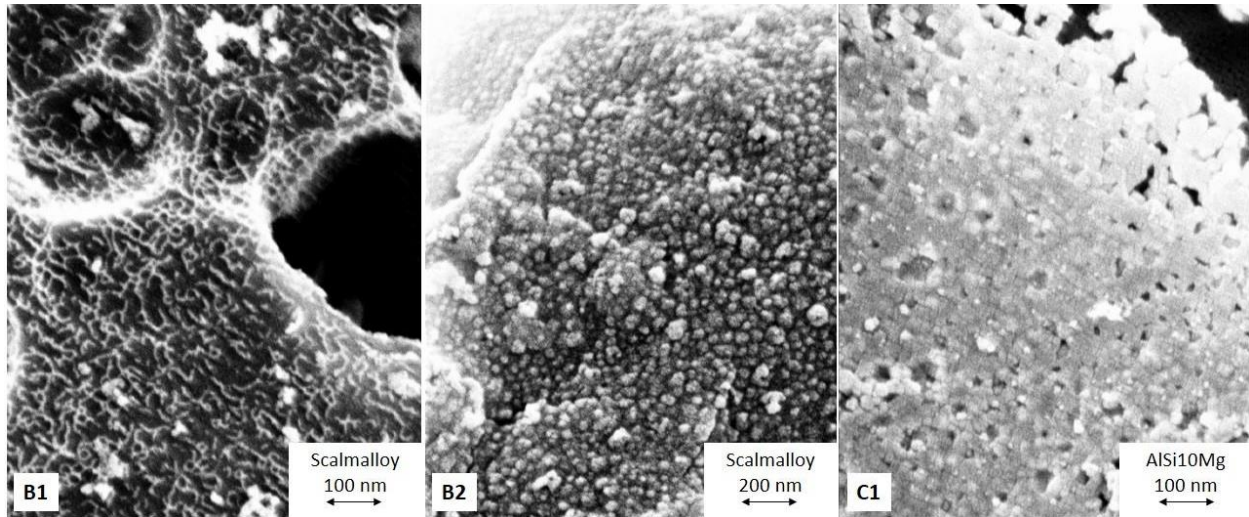
Figure A2: Images received from SEM. B1) Scalmalloy® at magnification 160 000x. B2) Scalmalloy® at magnification 300 000x. C1) AlSi10Mg at magnification 160 000x.

Appendix V – Profilometry values used in bar graph

The values used in the bar graphs in Figure 5.11, 5.12, 5.16 and 5.17. The Ra- and Rz-values were measured by a profilometer before and after the anodization step for all the samples. The percentage change before and after the anodization was also calculated.

Table A3. Standard deviation and calculation of Ra- and Rz values for the raw and blasted AM alloys before and after anodizing.

Surface structure	Value	Before anodizing [μm]	After anodizing [μm]	Percentage change [%]
2024-T3				
Raw	Ra	0.4 ± 0.05	0.5 ± 0.02	+ 17.5
	Rz	2.5 ± 0.2	3.6 ± 0.1	+ 46.2
Scalmalloy®				
Raw	Ra	8.3 ± 1.1	7.8 ± 0.6	- 6.6
	Rz	44.9 ± 5.9	41.9 ± 0.8	- 6.8
Blasted	Ra	5.6 ± 0.8	5.3 ± 0.6	- 5.7
	Rz	29.8 ± 3.0	26.8 ± 1.5	- 10.1
AlSi10Mg				
Raw	Ra	4.4 ± 1.1	4.1 ± 0.3	- 4.2
	Rz	26.4 ± 4.9	26.1 ± 2.5	- 1.1
Blasted	Ra	3.4 ± 0.4	3.3 ± 0.5	- 3.8
	Rz	20.0 ± 2.1	19.6 ± 2.3	- 1.9

The values used in the bar graphs in Figure 5.11, 5.12, 5.16 and 5.17. The Ra- and Rz-values were measured by a profilometer for all the different samples with different treatment.

Table A4. Calculated Ra- and Rz values for each alloy before and after anodizing.

Surface structure	Value	Anodized + powder	Anodized + primer + powder	Raw + powder	Raw + Adhesion promoter + powder
2024-T3					
Raw	*Ra*	0.3 ± *0.04*	0.3 ± *0.1*	0.2 ± *0.03*	0.3
	Rz	1.5 ± *0.07*	1.4 ± *0.3*	1.2 ± *0.03*	0.2
Scalmalloy®					
Raw	*Ra*	3.3 ± *0.4*	1.9 ± *0.8*	0.9 ± *0.3*	2.8
	Rz	15.6 ± *2.6*	8.1 ± *2.3*	3.5 ± *0.8*	12.9
Blasted	*Ra*	2.8 ± *1.2*	1.6 ± *0.7*	0.7 ± *0.2*	2.0
	Rz	10.3 ± *4.5*	5.9 ± *2.3*	3.1 ± *0.8*	8.6
AlSi10Mg					
Raw	*Ra*	1.3 ± *0.2*	0.2 ± *0.02*	0.3 ± *0.03*	0.8
	Rz	5.4 ± *1.4*	1.3 ± *0.03*	1.6 ± *0.04*	3.4
Blasted	*Ra*	0.6 ± *0.09*	0.3 ± *0.12*	0.4 ± *0.1*	1.0
	Rz	2.8 ± *0.1*	1.4 ± *0.16*	1.7 ± *0.5*	4.5

Table A5. *Calculated Ra- and Rz values for reference Scalmalloy$^{®}$after wet paint according to SAAB AB's standard..*

Surface structure	Value	Wet paint
Scalmalloy$^{®}$		
Raw	*Ra*	2.3 ± *1.0*
	Rz	10.7 ± *4.4*
Blasted	*Ra*	1.1 ± *0.3*
	Rz	4.4 ± *1.1*

Appendix VI - Supplementary material from ImageJ

The table below shows the calculated morphology parameters of samples anodized according to procedure 2.

Table A6. *Standard deviation and calculation of the pore diameter, interpore distance, pore wall thickness and porosity for the AM metals anodized according to procedure 2.*

Surface structure	Pore diameter [nm]	Interpore distance [nm]	Pore wall thickness [nm]	Porosity [%]
Scalmalloy/Raw	12.0 ± *2.9*	17.4 ± *2.3*	11.6 ± *6.7*	24.0 ± *1.2*
AlSi10Mg/Raw	10.2 ± *0.7*	26.6 ± *4.1*	19.0 ± *5.8*	15.7 ± *3.8*

Appendix VII - Last adhesion test

The last adhesion test performed on the powder coated samples.

Table A7. Results compiled from the last adhesion test

Sample	Results - comments
1. 2024-T3 Raw	-
2. Scalmalloy® Raw	No remark
3. AlSi10Mg Raw	No remark
4. 2024-T3 Anod.	No remark
5. Scalmalloy® Anod.	No remark
6. AlSi10Mg Anod.	No remark
7. 2024-T3 Anod. + primer	No remark
8. Scalmalloy® Anod. + primer	No remark
9. AlSi10Mg Anod. + primer	No remark

Appendix VIII - Timeline

During the first weeks of this master thesis, a planning report was written. The timeline, presented in Figure A3, was based on milestones and deadlines.

Time plan: AM Surface Treatment

Students	Karin Andersson and Marianne Gavelius
Supervisor	Linnea Selegård, Christian Ulrich, Zhangjun Hu
Date and version	2020-01-31, version 1.0

Project Week — Week 1 2 3 4 5 6 7 8 9 10 11 12 13 14 15 16 17 18 19 20 21
Calendar Week — Week 4 5 6 7 8 9 10 11 12 13 14 15 16 17 18 19 20 21 22 23 24

Nr	ACTIVITIES Description	Time Hours
1	Supervisor meeting	46
2	Litterature study	120
3	Writing planning report	40
4	Performing risk analysis	10
5	Laboratory introduction	12
6	Experimental design	80
7	Experimental work on anodic coatings	200
8	Experimental work on characterization	200
9	Experimental work on powder coating	200
10	Data analysis	80
11	Writing midterm report	80
12	Preparing midterm presentation	14
13	Writing final report	350
14	Preparing final presentation	40
15	Preparing presentation at Saab	14
16	Oppositioning	80
17	Writing reflection document	16
18	Extra time	18

DEADLINES
- Planning report
- Risk analysis
- Midterm report
- Midterm presentation
- Final report first draft
- Final report second draft
- Presentation at Saab
- Presentation at LiU
- Reflection document

HOLIDAYS
- Easter
- Walpurgis night
- Ascension day
- National day

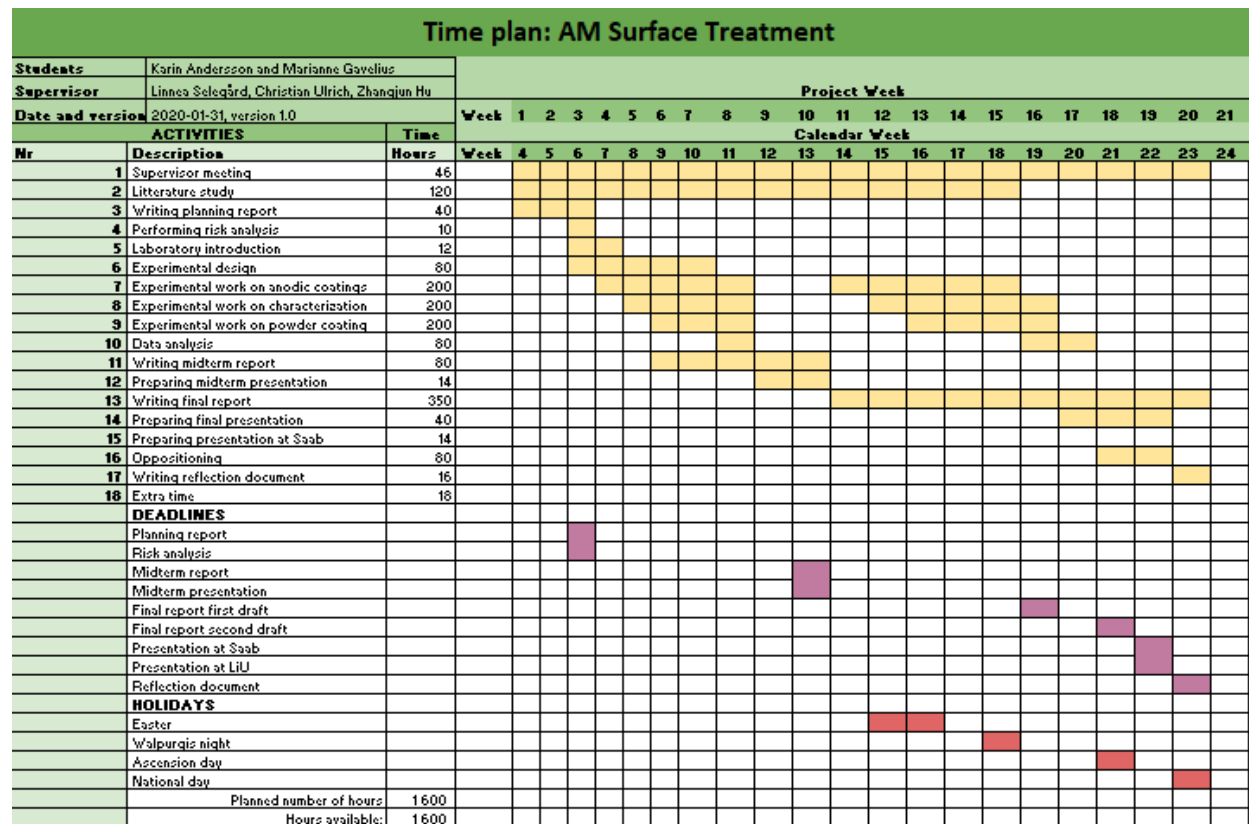|	
Planned number of hours	1600
Hours available:	1600

Figure A3: Time plan for the project. Created in the beginning of the project, January 2020.

69